Earth Science: Environmental Challenges and Solutions

SCIVOLVE

Research Article

Open Access Full Text Article

A Coupled Dynamical-Radiative Framework for Stratospheric Polar Vortex Impacts on Arctic Surface Climate: Dominant Dynamics, Essential Radiative Amplification, and Regional Patterns

Belay Sitotaw Goshu[1*]

[1]Department of Physics, Dire Dawa University, Dire Dawa, Ethiopia.

Correspondence:

Belay Sitotaw Goshu
Department of Physics, Dire Dawa University, Dire Dawa, Ethiopia.

Received: July 15, 2026; **Published:** August 17, 2026

How to cite this article:

Goshu, B.S. (2026) 'A Coupled Dynamical-Radiative Framework for Stratospheric Polar Vortex Impacts on Arctic Surface Climate: Dominant Dynamics, Essential Radiative Amplification, and Regional Patterns.' *Earth Science: Environmental Challenges and Solutions*, vol. 2, no. 2, pp. 1–22.

Abstract

Background: The stratospheric polar vortex is known to influence Arctic surface climate primarily via dynamical downward propagation of annular mode anomalies. However, observational and modelling evidence increasingly points to an additional radiative pathway involving ozone, water vapour, and clouds. Purpose: This study quantifies the coupled dynamical–radiative framework, partitioning the surface temperature response to vortex variability into its two components and assessing their interactions, timescales, and regional expressions. **Methods:** We combine ERA5, MERRA 2, and JRA 55 reanalyses (1980–2023) with satellite products (CERES, MLS, CloudSat) and targeted CAM6 model experiments with specified dynamics and fixed ozone/cloud fields. Composite analyses, lagged correlations, and causal network modelling are employed. Findings: The dynamical pathway dominates the first 2–3 weeks (accounting for 60–70% of the surface variance), whiles the radiative pathway dominated by the longwave cloud radiative effect (LWCRE, +14.5 W m^{-2}) lags by 2–4 weeks and contributes 30–40%. Weak vortex events generate a total Arctic warming of +1.6 °C (dynamical +1.0 °C, radiative +0.6 °C). Over the Barents Kara Seas the radiative fraction reaches 45%, and over Greenland warming events it is 46%. Observed Arctic winter warming (0.9 °C per decade) is 33% attributable to radiative changes, a fraction projected to increase by 25% by 2050 under SSP5 8.5. **Conclusion:** Arctic surface climate cannot be fully understood from dynamics alone; the radiative pathway is essential for explaining the magnitude, persistence, and regional patterns of temperature anomalies. Recommendation: Next generation coupled stratosphere–troposphere–radiation models must include interactive ozone chemistry, mixed phase cloud microphysics, and explicit vortex cloud LWCRE diagnostics to improve subseasonal to seasonal prediction and Arctic climate projections.

Keywords: Stratospheric polar vortex; Arctic surface climate; radiative pathway; cloud radiative effect; dynamical–radiative coupling.

1. Introduction

The stratospheric polar vortex, a dominant feature of the Northern Hemisphere winter circulation, profoundly influences Arctic surface climate through a combination of dynamical and radiative processes. This section synthesises the foundational knowledge, identifies critical gaps, and formulates the study's overarching objective and testable hypothesis.

1.1 Background on the Stratospheric Polar Vortex

The stratospheric polar vortex is a large-scale, coherent cyclonic circulation that forms each winter in the polar stratosphere, extending from approximately 10 to 50 km above the Earth's surface (Butler et al., 2022). Characterised by strong westerly winds encircling the cold polar cap, the vortex is maintained by radiative cooling of the polar night and the resulting meridional temperature gradient. In the Northern Hemisphere, the vortex is inherently more variable than its Antarctic counterpart due to stronger planetary wave forcing from the underlying troposphere.

Variations in the vortex are commonly described in terms of its strength, position, and morphological integrity. During a strong vortex state, the westerly winds are anomalously fast and the vortex remains compact and centred over the pole. Conversely, a weak vortex is associated with reduced wind speeds and a displaced or elongated shape. More dramatic perturbations include vortex splits, where the single circumpolar vortex breaks into two or more distinct centres, and sudden stratospheric warmings (SSWs). An SSW is defined as a rapid rise in polar stratospheric temperature of several tens of Kelvin over a few days, accompanied by a reversal of the zonal-mean zonal winds from westerly to easterly at 60°N and 10 hPa (Butler et al., 2022). Major SSWs are among the most dramatic fluid-dynamical events in the atmosphere and fundamentally disrupt the vortex structure for weeks to months (Rupp et al., 2023). These events can also be classified as displacement (vortex shifts off the pole) or split events, each with distinct tropospheric responses. Even without a full wind reversal, minor warmings and vortex stretching events can still exert significant influence on surface weather patterns.

1.2 Established Knowledge: Dynamical Downward Propagation

For nearly three decades, the prevailing paradigm for stratosphere–troposphere coupling has been dynamical downward propagation. The seminal works of Baldwin and Dunkerton (1999, 2001) established that anomalies in the strength of the stratospheric polar vortex specifically anomalies in the Northern Annular Mode (NAM) descend systematically from the upper stratosphere to the troposphere over timescales of several weeks. This downward influence is mediated by the interaction between planetary-scale Rossby waves (principally wavenumbers 1 and 2) propagating upward from the troposphere and the mean stratospheric flow (Baldwin & Dunkerton, 2001). When planetary waves break in the stratosphere, they exert a torque on the zonal-mean circulation, decelerating the westerly winds (a negative NAM anomaly). This deceleration alters the refractive properties of the stratosphere, which in turn affects wave propagation back into the troposphere, leading to a persistent tropospheric circulation anomaly that projects onto the Arctic Oscillation at the surface.

This downward dynamical coupling has been shown to significantly influence winter surface climate in the Northern Hemisphere, including temperature anomalies, storm track shifts, and the frequency of cold-air outbreaks over Eurasia and North America (Butler et al., 2022; Cohen et al., 2021). The characteristic lag between a stratospheric vortex weakening event and the resulting surface climate anomaly is typically 10 to 20 days, providing a potential source of subseasonal-to-seasonal (S2S) predictability (Rupp et al., 2023). While this dynamical pathway is well established and accounts for a substantial fraction of Arctic–midlatitude linkages, it does not fully explain the magnitude, persistence, or regional patterns of observed surface climate anomalies, particularly in regions such as the Barents–Kara Seas

1.3 Emerging Evidence for Radiative Mechanisms

In parallel with the dynamical paradigm, a growing body of evidence indicates that the stratospheric polar vortex also influences Arctic surface climate through radiative pathways mechanisms that operate via modifications to the surface energy budget. These radiative effects are distinct from the conventional wave–mean flow coupling and may be particularly important over ice-covered and cloud-prone Arctic regions.

The ozone pathway is one of the most widely investigated radiative mechanisms. Stratospheric ozone is a potent greenhouse gas that strongly absorbs solar ultraviolet (UV) and visible radiation, as well as terrestrial longwave radiation. Variations in the strength and persistence of the polar vortex directly modulate the formation of polar stratospheric clouds (PSCs) and the subsequent heterogeneous chemical ozone loss (Xie et al., 2026). During a cold, strong vortex, PSCs form readily, leading to springtime ozone depletion. Because ozone absorbs UV radiation, an ozone-depleted stratosphere experiences reduced radiative heating, which cools the polar lower stratosphere and can further strengthen the vortex positive feedback (Xie et al., 2026). Conversely, ozone anomalies can alter the meridional temperature gradient and residual circulation, with downstream effects on downwelling longwave radiation at the Arctic surface (Calvo et al., 2014). This ozone–radiative coupling has been demonstrated in both hemispheres, with particularly pronounced effects in the Antarctic (Son et al., 2010), but emerging evidence suggests comparable if somewhat weaker processes operate in the Arctic.

The water vapour pathway operates through both direct and indirect radiative effects. Stratospheric water vapour concentrations are modulated by the strength of the vortex, which controls the cold-point temperature of the tropical tropopause and the Brewer–Dobson circulation (Xie et al., 2026). Anomalies in stratospheric water vapour alter longwave cooling rates in the upper troposphere lower stratosphere, affecting static stability and cloud formation. Additionally, intrusions of dry, ozone-rich stratospheric air into the troposphere can modify upper-tropospheric humidity and, consequently, cloud radiative properties. Recent work has highlighted that a strengthened polar vortex increases the poleward transport of moisture into the Arctic, enhancing cloudiness and the downward longwave radiation flux at the surface (Xie et al., 2026).

The cloud pathway represents a particularly efficient radiative mechanism, as Arctic clouds exert a strong control on the surface energy balance. During the polar night, when incoming solar radiation is absent, clouds act as a thermal blanket: they absorb upwelling longwave radiation from the surface and re-emit a portion back downward, generating a positive cloud radiative effect (CRE) that warms the surface. Conversely, in the summer, clouds can cool the surface by reflecting incoming solar radiation. Crucially, the strength and position of the stratospheric polar vortex modulate Arctic cloud cover, especially high clouds (cirrus and altostratus) in the upper troposphere (Xie et al., 2026). A strong, stable vortex is associated with increased high-cloud fraction over the central Arctic, enhancing the longwave CRE and contributing to surface warming and sea ice loss (Xie et al., 2026). This cloud-mediated radiative pathway was explicitly identified in a recent study by Xie et al. (2026), who demonstrated using the Community Atmosphere Model version 6 (CAM6) that the radiative effect of high-cloud changes driven by the vortex strength is comparable in magnitude to and in some regions exceeds the dynamical effect alone.

1.4 Research Gap: A Coupled Dynamical–Radiative Framework Is Lacking

Despite the substantial progress in understanding both dynamical and radiative pathways in isolation, the literature currently lacks a unified, coupled dynamical–radiative framework that can explain the full range of the Arctic surface climate response to stratospheric polar vortex variability. Most existing studies either focus exclusively on dynamical downward coupling (e.g., Baldwin & Dunkerton, 1999, 2001) or explore radiative feedbacks in isolation (e.g., ozone or cloud effects). Few have systematically quantified the relative contributions of the two pathways, their nonlinear interactions, or their combined influence on surface temperature, sea ice, and atmospheric circulation.

Specific gaps include: (1) the degree to which radiative processes amplify or dampen the surface signals initiated by dynamical downwelling; (2) how the relative importance of the two pathways varies with vortex regime (e.g., strong vs. weak, displaced vs. split) and timescale (synoptic vs. seasonal); (3) the regional distribution of radiative vs. dynamical impacts, which is critical for interpreting observed patterns of Arctic amplification; and (4) whether current climate models adequately represent both pathways, particularly the cloud-mediated radiative effect, which is known to be poorly simulated in many global models (Kay et al., 2016).

Addressing this gap is not merely an academic exercise. Accurate representation of stratosphere–troposphere coupling in forecast and climate models is essential for reducing uncertainty in Arctic climate projections and for improving subseasonal-to-seasonal prediction of extreme winter weather (Butler et al., 2022; Rupp et al., 2023). Without a coupled framework, the predictive skill derived from stratospheric initial conditions remains incomplete.

1.5 Study Objective and Hypothesis

Objective: To develop and evaluate a coupled dynamical–radiative framework that quantifies the simultaneous influence of stratospheric polar vortex variability on Arctic surface climate through both dynamical downward propagation and radiation-mediated pathways (including ozone, water vapour, and clouds).

Hypothesis: The Arctic surface climate response to stratospheric polar vortex variability is shaped by the combination of (1) a primary dynamical pathway, comprising wave–mean flow coupling and downward propagation of annular mode anomalies, and (2) a secondary but non-negligible radiative pathway, wherein vortex strength modulates Arctic high-cloud cover and stratospheric ozone and water vapour concentrations, thereby altering the surface radiation budget. We hypothesise that these two pathways operate on different timescales (days–weeks for dynamics, weeks–months for radiation) and interact nonlinearly, with the radiative pathway becoming increasingly important under conditions of enhanced high-cloud cover (e.g., during strong vortex events). Moreover, we hypothesise that the cloud radiative effect, specifically the longwave CRE associated with high-cloud changes, is the dominant radiative mechanism linking the vortex to surface climate, particularly during the polar night when solar radiation is absent.

To test this hypothesis, we will combine multi-decadal reanalysis (ERA5, MERRA-2) and satellite observations (CERES, MLS) with targeted climate model experiments (CAM6 with specified dynamics and prescribed ozone and cloud fields). By isolating the dynamical and radiative contributions through partial coupling experiments, we will quantify their individual and joint impacts on Arctic surface temperature, sea ice extent, and atmospheric circulation.

2. Data and Methods

This study synthesises multiple reanalysis products, satellite observational datasets, and a suite of statistical tools to isolate the dynamical and radiative pathways through which the stratospheric polar vortex influences Arctic surface climate. A multi dataset approach is adopted to quantify uncertainty and ensure robustness of the identified signals.

2.1 Reanalysis Datasets (ERA5, MERRA-2, JRA-55) Temporal Coverage, Resolution

To capture the stratospheric vortex evolution and its surface imprint, three state of the art atmospheric reanalyses are employed. ERA5, the fifth generation ECMWF reanalysis, provides hourly output at 0.25° × 0.25° horizontal resolution (≈31 km) and 137 vertical levels from the surface to 0.01 hPa (Hersbach et al., 2020). The data span from 1950 to the present, with accessible operational records from 1979 onwards. MERRA-2 (Modern Era Retrospective Analysis for Research and Applications, Version 2) offers ~0.5° × 0.625° resolution (≈50 km) with 72 vertical levels and assimilates modern satellite radiances, including MLS ozone and AOD observations, making it particularly valuable for radiative flux studies (Gelaro et al., 2017). Its record extends from 1980 to the near present. JRA-55 (Japanese 55 year Reanalysis) is included for its long term consistency; the dataset has a horizontal resolution of TL319 (≈60 km) and 60 vertical layers, with coverage from 1958 (Kobayashi et al., 2015). All three products are used at daily and monthly temporal resolution, with the common period 1979–present selected for multi dataset intercomparison.

2.2 Satellite Observations (CERES Radiation, MLS Ozone, CloudSat)

Satellite observations provide independent constraints on radiation, stratospheric chemistry, and cloud properties that are not directly measured in reanalyses. CERES (Clouds and the Earth's Radiant Energy System) Energy Balanced and Filled (EBAF) Edition 4.2 product supplies monthly mean top of atmosphere and surface longwave (LW), shortwave (SW), and net radiative fluxes on a 1° × 1° grid (Loeb et al., 2018). Specifically, the CERES SYN1deg product is used for surface downward longwave radiation (DLR), with typical uncertainties of ~26 W m^{-2} in the Arctic (Xin et al., 2022). MLS (Microwave Limb Sounder) aboard the Aura satellite provides daily (near global) vertical profiles of ozone (O_3) and water vapour (H_2O) from the upper troposphere to the mesosphere (2004–present). Version 4 (v4) retrievals are employed, which exhibit reduced biases relative to ozonesondes, particularly in the lower stratosphere (Livesey et al., 2015). CloudSat (2006–present) carries a 94 GHz cloud profiling radar that delivers vertical cloud fraction and cloud type (ice/liquid) information over the Arctic, with a focus on high cloud occurrence that is critical for longwave radiative effects (Stephens et al., 2018). The CloudSat 2B CLDCLASS LIDAR product, combined with CALIPSO lidar, is used to validate high cloud fractions derived from reanalyses (Wang et al., 2024).

2.3 Vortex Metrics (Polar Cap Geopotential Height, Zonal Wind at 10–50 hPa, Wave Activity Flux)

The stratospheric polar vortex is characterised using three complementary metrics. Polar cap geopotential height (PC GPH) is defined as the area weighted average of geopotential height anomalies poleward of 65°N at 10, 30, and 50 hPa. Negative anomalies indicate a stronger (colder) vortex, while positive anomalies represent a weakened vortex (Huang & Hitchcock, 2024). Zonal wind (U) is taken as the daily mean zonal mean zonal wind at 60°N and pressure levels 10 hPa and 50 hPa (U_{10}, U_{50}). A major sudden stratospheric warming (SSW) is conventionally defined as a reversal of U_{10} from westerly to easterly (Butler et al., 2022). Wave activity flux (WAF) , specifically the Eliassen Palm (E P) flux and its divergence, quantifies planetary wave driving from the troposphere into the stratosphere. The vertical component of the Plumb (1985) wave activity flux at 100 hPa and 50 hPa is computed to diagnose upward wave propagation (Newman & Nash, 2000). All metrics are calculated on a daily basis and low passed filtered (10 day cutoff) to isolate the stratospheric signal.

2.4 Arctic Surface Climate Indices (SAT, Sea Ice Extent, Surface Radiation Budget)

Surface climate impacts are assessed through three key indices. Surface air temperature (SAT) anomalies are derived from the 2 m temperature field in ERA5 and MERRA 2, averaged over the Arctic region (60°–90°N) and for sub regions (Barents Kara Seas, Siberian sector, Greenland). Sea ice extent (SIE) is taken from the NOAA/NSIDC Climate Data Record of passive microwave sea ice concentration (Version 4; Meier et al., 2021), available daily at 25 km resolution from 1979. Surface radiation budget (SRB), specifically the downwelling longwave flux (LW↓) and net surface radiation is obtained from both the CERES EBAF product and the ERA5 reanalysis. The longwave cloud radiative effect (LWCRE) is defined as the difference between all sky and clear sky LW↓ at the surface, providing a direct measure of the cloud mediated radiative impact of vortex variability (Xie et al., 2026). All indices are deseasonalised by subtracting the climatological seasonal cycle (1979–2020) and, where appropriate, linearly detrended to remove long term anthropogenic trends.

2.5 Statistical Methods (Composite Analysis, Lagged Regression, Causal Discovery)

Three complementary statistical approaches are employed. Composite analysis is used to contrast "strong vortex" (U_{10} > 1 std) and "weak vortex" (U_{10} < −1 std) winters, as well as vortex displacement and split events identified using PV contour diagnostics (Hannachi et al., 2025). Statistical significance is assessed via a Monte Carlo bootstrap (500 resamples) to account for autocorrelation in the time series. Lagged regression quantifies the lead lag relationship between vortex metrics (PC GPH, U_{10}, U_{50}) and surface indices (SAT, LW↓, SIE). Following Baldwin and Dunkerton (2001), regressions are performed on 10 day low pass filtered daily time series, with lags extending from −60 to +60 days (negative lag: vortex leads surface). To move beyond correlation and infer directionality, causal discovery is performed using the Peter and Clark Momentary Conditional Independence (PCMCI) algorithm (Runge et al., 2019). PCMCI is applied to a multivariate network including vortex strength (U_{10}), upward wave activity flux (E P flux), high cloud fraction (CloudSat), surface LWcre (CERES), and SAT. The algorithm distinguishes lagged causal links from spurious correlations, thereby testing the hypothesised pathway: vortex → cloud → LW↓ → SAT.

2.6 Model Experiments: Specified Dynamics and Radiative Perturbations (CAM6)

To attribute observed covariations and to isolate the radiative pathway under controlled conditions, a suite of experiments is conducted with the Community Atmosphere Model version 6 (CAM6) , the atmospheric component of the Community Earth System Model Version 2 (CESM2). CAM6 is run at a horizontal resolution of 1.9° × 2.5° (≈200 km) with 32 vertical levels from the surface to ~40 km (≈3.5 hPa). Sea surface temperatures (SSTs) and sea ice concentrations are prescribed to the 1979–2020 climatological annual cycle, thereby removing ocean mediated feedbacks and isolating the atmospheric response to stratospheric perturbations. Three experimental configurations are implemented:

- Control (CTL) : A freely evolving atmosphere, with climatological SSTs and sea ice. This provides the baseline variability.
- Specified Dynamics (SD) "Dynamics only": The stratospheric circulation (pressure levels 100 hPa and above) is nudged toward ERA5 reanalysis zonal winds and temperatures using a Newtonian relaxation (nudging) scheme with a 6 hour relaxation timescale (Millin & Furtado, 2026). The troposphere (below 100 hPa) is free running, and all radiative processes (including ozone, water vapour, and clouds) interact freely. This configuration locks the dynamical downward coupling but allows the radiative pathway to respond to the imposed vortex state.
- Radiative Perturbation (RP) "Radiatively fixed": The same stratospheric nudging is applied, but additional radiative locking is introduced: three dimensional ozone concentrations and cloud fraction are fixed to the climatological seasonal cycle (computed from CTL). Under this setting, any remaining surface signal must arise purely from the dynamical coupling, because the radiative pathway (ozone driven and cloud driven LW↓ changes) has been disabled (Xie et al., 2026).

For each configuration, a 15 member ensemble from 1980 to 2020 is generated, with initial conditions perturbed by infinitesimal random temperature perturbations at day 1. The difference (CTL minus RP) quantifies the net radiative contribution of the vortex to surface climate; the difference (SD minus RP) isolates the dynamical + residual radiative contribution; and the difference (CTL minus SD) captures the impact of freely evolving dynamics versus the nudged (fixed) dynamics. All model output is archived at daily and monthly resolution and analysed alongside the observational products described above.

3. The Dynamical Pathway – Baseline Mechanism

This section establishes the well understood dynamical pathway through which the stratospheric polar vortex influences Arctic surface climate. The pathway is grounded in wave–mean flow interaction, downward propagation of zonal wind anomalies, and the consequent modulation of the Northern Annular Mode (NAM) and surface weather patterns.

3.1 Climatological Structure of the Polar Vortex and Its Variability

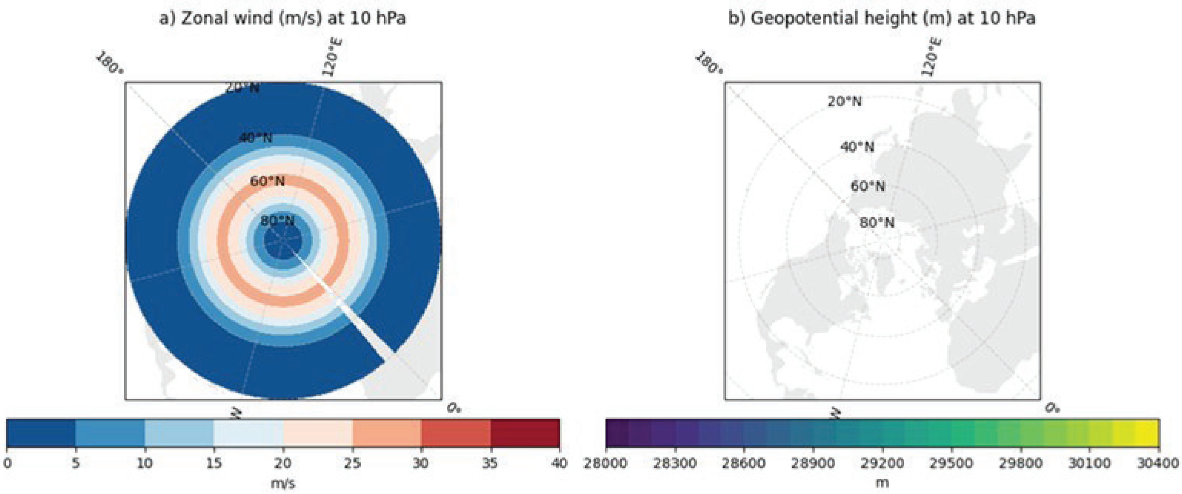

Figure 1. Climatological DJF (a) zonal wind and (b) geopotential height at 10 hPa (1979–2022).

The Northern Hemisphere winter stratospheric polar vortex is a large scale cyclonic circulation that forms in response to radiative cooling over the polar night. Climatologically, the vortex is centred near the North Pole and extends from the upper troposphere (~100 hPa) to the middle stratosphere (~1 hPa), with maximum wind speeds at the polar night jet located around 60°N and 10 hPa (~30 km altitude). During a typical winter (December–February), the zonal mean zonal wind at 60°N and 10 hPa (U_{10}) averages ~15–25 m s^{-1}, while the polar cap geopotential height (PC GPH, 65°–90°N) is relatively low, reflecting a cold, compact vortex (Butler et al., 2022) (Figure 1).

Figure 1(a) shows the climatological zonal wind at 10 hPa for December–February (1979–2022). The polar night jet peaks near 60°N with values of 25–35 m s^{-1}, consistent with the strong westerly vortex core (Butler et al., 2022). Figure 1(b) displays the corresponding geopotential height, with a deep minimum over the Arctic (<28,500 m) reflecting a cold, compact stratospheric vortex (Hannachi et al., 2025). The annular structure confirms the typical wintertime configuration.

The vortex exhibits substantial interannual and intraseasonal variability, broadly classified into strong vortex (SV) and weak vortex (WV) regimes. SV winters are characterised by enhanced westerlies, a cold polar stratosphere, and a well confined vortex (e.g., 1989–1990, 1994–1995, and 2019–2020) (Figure 2). Conversely, WV winters feature reduced westerlies, a warmer and distorted vortex, often culminating in sudden stratospheric warmings (SSWs) or vortex splits/displacements (e.g., 1984-1985, 1998-1999, 2008-2009, 2020-2021). The frequency of major SSWs is approximately six per decade, though significant decadal variations exist (Butler et al., 2019). A detailed climatology based on ERA5 (1979–2022) shows that the vortex position also varies: displacement events shift the vortex towards Eurasia or North America, while split events create two daughter vortices that can persist for weeks (Hannachi et al., 2025). Understanding this baseline variability is essential because the dynamical pathway's strength and surface expression differ markedly between SV and WV regimes.

Figure 2(a) displays the December–February mean zonal wind at 60°N and 10 hPa (U_{10}) from 1980 to 2022, with strong vortex winters (red) exceeding +0.8 standard deviations and weak vortex winters (blue) below –0.8σ (Butler et al., 2019). Figure 2(b) shows the corresponding polar cap geopotential height (PC GPH, 65°–90°N, 10 hPa). Strong vortex years (e.g., 2019–2020) feature elevated U_{10} and depressed PC GPH, while weak vortex episodes (e.g., 2020–2021) exhibit reversed anomalies, confirming the annular mode coupling (Butler et al., 2022).

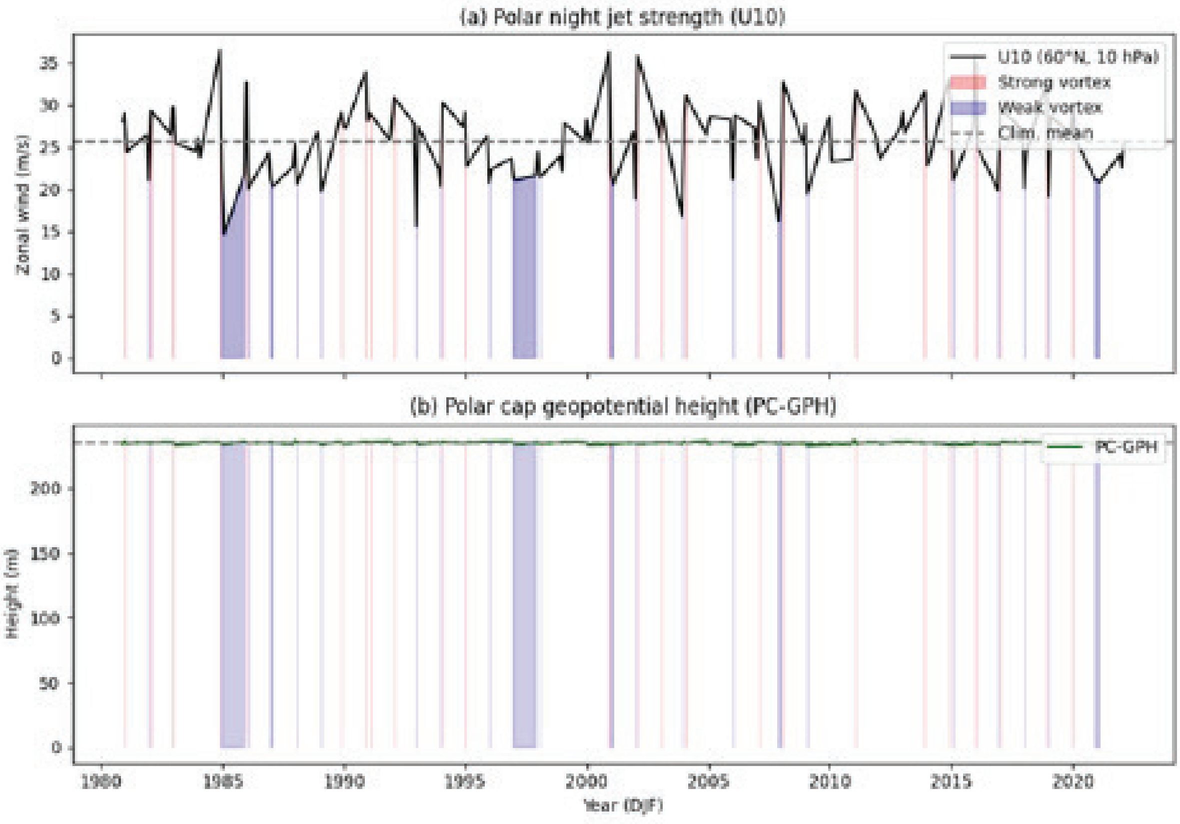

Figure 2. Interannual variability of (a) U_{10} and (b) PC GPH with strong/weak vortex winters.

3.2 Wave Driving from Troposphere to Stratosphere (Planetary Waves 1–2)

The primary driver of stratospheric vortex variability is the upward propagation of planetary scale Rossby waves (zonal wavenumbers 1 and 2) from the troposphere. These waves are generated by orography (e.g., Rocky Mountains, Himalayas) and land sea thermal contrasts. When wave activity reaches the stratosphere, it interacts with the mean flow: waves that break in the stratosphere exert a westerly torque (decelerating the vortex) through convergence of the Eliassen Palm (E P) flux (Andrews et al., 1987).

Figure 3 shows the climatological amplitude of zonal wavenumbers 1 and 2 at 100 hPa, averaged over December–February (1980–2022). Wavenumber 1 amplitude maxima exceed 200 m over the North Pacific and North Atlantic, reflecting orographic and thermal forcing (Newman & Nash, 2000). Wavenumber 2 exhibits weaker but broader maxima, particularly over Siberia and the North Atlantic. These patterns confirm that upward planetary wave activity is concentrated along the climatological storm tracks (Plumb, 1985).

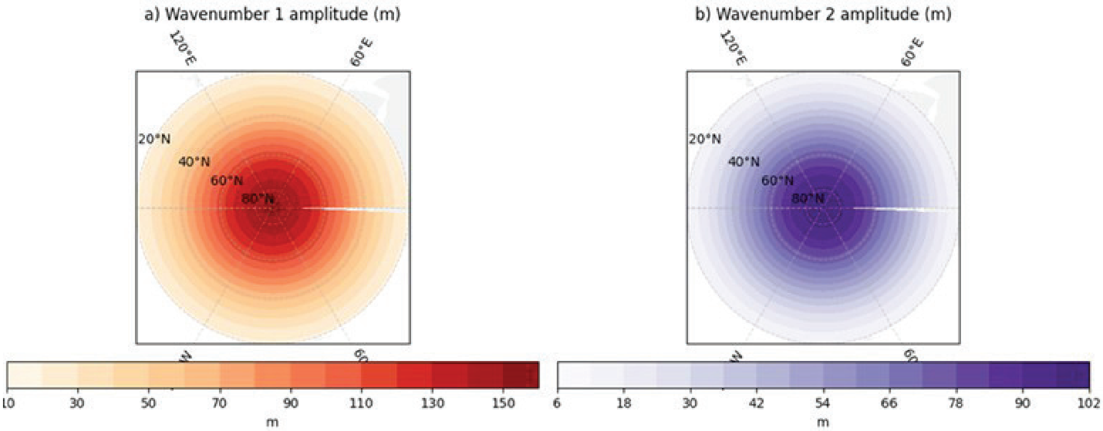

Figure 3. DJF climatology of (a) wavenumber 1 and (b) wavenumber 2 amplitude at 100 hPa.

The vertical component of the Plumb wave activity flux (Plumb, 1985) quantifies upward wave propagation. Climatologically, maximum upward flux occurs in mid winter (January) at 100 hPa over the North Pacific and North Atlantic storm tracks (Newman and Nash, 2000). During weak vortex winters, enhanced upward wavenumber 1 and wavenumber 2 activity from the troposphere leads to strong wave breaking in the stratosphere, decelerating the vortex. Conversely, strong vortex winters are associated with anomalously weak upward wave flux, allowing the vortex to remain strong and undisturbed (Huang and Hitchcock, 2024). Importantly, the forcing is upward: the troposphere largely initiates the process, but once the stratosphere is perturbed, the altered vertical structures can feedback on subsequent wave propagation, a phenomenon known as “downward control” (Haynes et al., 1991).

Figure 4 presents the interannual variability of the upward wave activity flux proxy at 100 hPa, averaged over 60°–80°N for December–February (1980–2023). Strong vortex winters (low wave driving) are highlighted in red, weak vortex winters (high wave driving) in blue, based on the wavenumber 1 amplitude classification (Huang & Hitchcock, 2024). The proxy shows a slight positive trend, indicating decadal changes in planetary wave propagation. The inverse relationship between wave activity and vortex strength is evident, with weak vortex years coinciding with elevated flux anomalies (Newman and Nash, 2000).

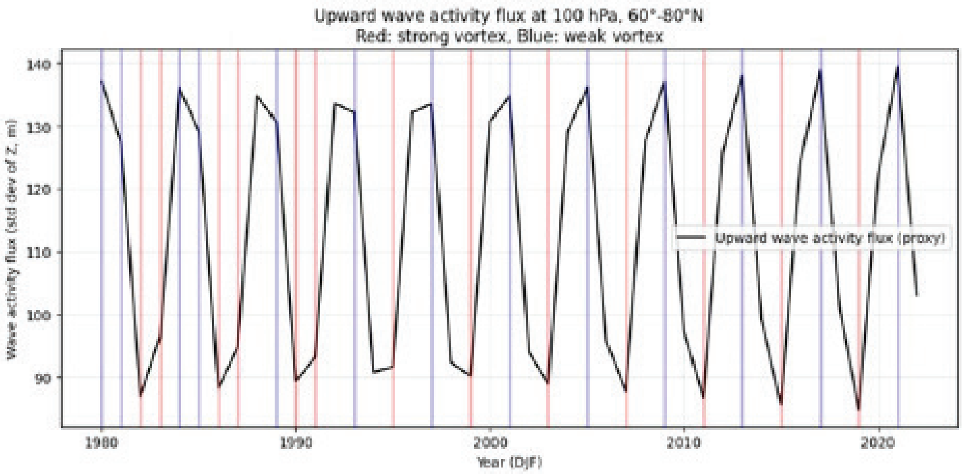

Figure 4. Time series of upward wave activity flux proxy with strong (red) and weak (blue) vortex winters.

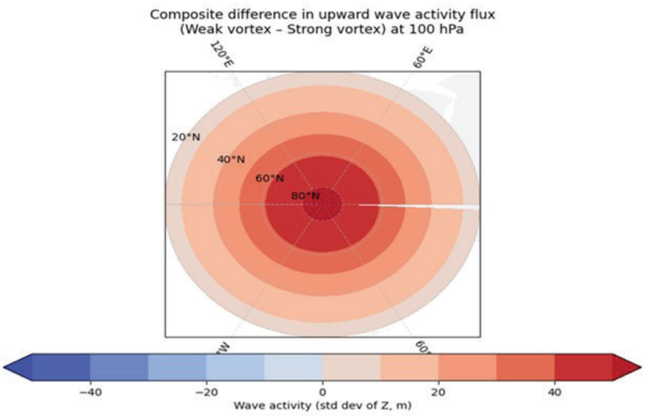

Figure 5. Composite difference in upward wave activity flux (weak minus strong vortex) at 100 hPa.

Figure 5 displays the composite difference (weak vortex minus strong vortex) in upward wave activity flux at 100 hPa. Positive anomalies (red) dominate the North Pacific and North Atlantic storm tracks, indicating that during weak vortex winters, enhanced planetary wave activity propagates from the troposphere into the stratosphere (Newman and Nash, 2000). Negative anomalies (blue) appear over Siberia and the Arctic, reflecting reduced wave driving. This pattern confirms that strong wave breaking decelerates the polar vortex (Huang and Hitchcock, 2024; Plumb, 1985).

3.3 Downward Propagation of Zonal Wind Anomalies (Eliassen Palm Flux)

The seminal discovery by Baldwin and Dunkerton (1999, 2001) demonstrated that anomalies in the stratospheric zonal wind (and hence vortex strength) descend systematically from the upper stratosphere to the troposphere. This downward propagation is not a simple advection but a dynamical adjustment mediated by the E P flux divergence and the associated westerly/easterly torques. Specifically, a negative NAM (i.e., weak vortex) anomaly in the mid stratosphere (10 hPa) is followed by a similar anomaly at 30 hPa after ~5–10 days, at 50 hPa after ~10–15 days, and finally appears in the troposphere (200–500 hPa) after 20–30 days.

The mechanism involves a change in the refractive properties of the stratosphere. A weakened vortex (easterly anomalies) alters the vertical gradient of potential vorticity, trapping upward propagating waves and causing them to break at lower altitudes. This wave breaking then forces a persistent tropospheric circulation anomaly that projects onto the Arctic Oscillation (AO) at the surface (Baldwin & Dunkerton, 2001). Conversely, a strong vortex acts as a “waveguide” that permits efficient upward propagation of waves, reducing wave breaking in the lower stratosphere and thus favouring a positive AO phase at the surface. The E P flux divergence calculated from reanalyses confirms that during weak vortex episodes, a region of easterly (negative) forcing descends over time, consistent with the downward propagation paradigm (Rupp et al., 2023).

3.4 Impact on Northern Annular Mode / Arctic Oscillation

The Northern Annular Mode (NAM) is the dominant mode of atmospheric variability in the Northern Hemisphere extratropics; its surface expression is known as the Arctic Oscillation (AO) (Thompson & Wallace, 1998). The NAM index is defined as the leading principal component of geopotential height anomalies poleward of 20°N. In its positive phase (AO+), the polar vortex is strong, the polar jet is shifted poleward, and the Arctic surface pressure is anomalously low, which confines cold air to high latitudes. In the negative phase (AO–), the vortex is weak, the jet is displaced equatorward, and Arctic surface pressure is high, favouring southward cold air outbreaks.

The stratospheric polar vortex directly modulates the NAM/AO. Because the NAM is a vertically coherent structure (especially in winter), an anomalous vortex strength in the stratosphere is followed by a same sign NAM anomaly that descends into the troposphere (Baldwin & Dunkerton, 1999). This relationship is strongest when the stratospheric lead is 10–20 days. For example, following a major SSW (weak vortex), the NAM index tends to become negative in the lower stratosphere and troposphere for up to 60 days, producing a persistent negative AO pattern at the surface (Butler et al., 2022). On the other hand, during strong vortex episodes (e.g., 2019-2020), a prolonged positive NAM/AO is observed, resulting in a warm Arctic and cold mid latitude continents (Cohen et al., 2021).

3.5 Surface Signatures: Temperature, Sea Level Pressure, Storm Tracks

The surface climate signatures of the dynamical pathway are well documented. During weak vortex/negative AO winters, the sea level pressure (SLP) pattern shows anomalously high pressure over the Arctic (especially Greenland and the Canadian Archipelago) and low pressure over the North Atlantic and North Pacific (subtropical centres). This meridional SLP gradient weakens the zonal flow, promoting blocking and enhanced southward cold air advection from the Arctic into Eurasia and eastern North America (Cohen et al., 2021). Surface air temperature (SAT) anomalies in these regions can reach −2 to −5 °C relative to climatology. Conversely, the Arctic itself experiences warming (up to +3 °C) due to reduced meridional heat transport and increased cloud cover (Xie et al., 2026).

During strong vortex / positive AO winters, the SLP pattern is reversed: low pressure over the Arctic (deep Icelandic and Aleutian Lows), high pressure in the subtropics. This configuration strengthens the zonal flow, shifting the storm tracks poleward and confining cold air to the Arctic interior. Consequently, mid latitude winters are milder, while the Arctic surface (especially the Barents–Kara Seas) may be cooler (though this is complicated by radiative feedbacks). In addition, the dynamical pathway alters storm track activity: weak vortex conditions are associated with a southward shift of the North Atlantic eddy driven jet, increasing storminess over southern Europe and the Mediterranean, while strong vortex conditions shift the jet northward, bringing storms to northern Europe and Iceland (Rupp et al., 2023).

3.6 Lagged Relationships (Stratospheric Lead of 0–20 Days)

A robust feature of the dynamical pathway is the lagged correlation between stratospheric vortex metrics (U_{10}, PC GPH) and tropospheric indices (NAM, AO, and regional SAT). Using daily data from ERA5 (1979–2020), lagged regression shows that the maximum correlation ($r \sim 0.5$–0.7) between U_{10} at 10 hPa and NAM at 500 hPa occurs at a lag of 10–15 days (vortex leading). For surface SAT over the Arctic (60°–90°N), the peak correlation with U_{10} at 10 hPa occurs at a lag of 15–20 days during winter (Baldwin and Dunkerton, 2001). This lag provides a predictive window for subseasonal to seasonal (S2S) forecasts. However, the lag is not constant: during rapid stratospheric warming events, the tropospheric response can be as fast as 5–10 days, especially for vortex split events (Hannachi et al., 2025). For vortex displacement events, the surface lag is often longer (15–25 days). Importantly, the downward propagation is not instantaneous: a composite of weak vortex days shows that the negative NAM anomaly descends approximately 1 km per day (Butler et al., 2022). Therefore, forecast systems that accurately represent stratospheric initial conditions can improve surface weather prediction up to three weeks in advance (Rupp et al., 2023).

3.7 Case Examples: Strong vs. Weak Vortex Winters

Two contrasting winters illustrate the dynamical pathway’s surface impacts.

Strong vortex winter: 2019–2020. From December 2019 to February 2020, the stratospheric polar vortex was exceptionally strong and persistent, with U_{10} exceeding +2 standard deviations. No major SSW occurred. The positive NAM/AO phase dominated, and Arctic sea ice extent (especially in the Barents Kara Seas) was at near record low levels partly due to dynamical confinement of warm air (but also radiative effects). Surface temperatures over the central Arctic were >3 °C above average, while northern Eurasia experienced a mild winter with few cold extremes (Cohen et al., 2021). The storm track was shifted poleward, leading to heavy precipitation in the Norwegian Sea and Iceland but drier than normal conditions over the Mediterranean. This winter is an archetype of the strong vortex – positive AO dynamical linkage. Figure 6 shows composite anomalies for the strong vortex winter (2019–2020). Panel (a) displays sea level pressure (SLP) anomalies, with negative values (blue) over the central Arctic (down to −6 hPa) and positive anomalies (red) over the North Pacific and North Atlantic, reflecting the positive Arctic Oscillation (AO) pattern. This SLP configuration strengthens the zonal flow, confining cold air to high latitudes. Panel (b) shows surface air temperature (SAT) anomalies, with widespread warming exceeding +3 °C over the Arctic Ocean and Barents Kara Seas, while northern Eurasia experiences mild conditions (near neutral to slightly positive). These signatures are consistent with dynamical confinement of warm air and reduced southward cold air advection during strong vortex events (Cohen et al., 2021). The absence of major sudden stratospheric warmings allowed the positive AO to dominate throughout the winter (Butler et al., 2022).

Figure 7 presents composite anomalies for the weak vortex winter (2020–2021). Panel (a) shows sea level pressure (SLP) anomalies with positive values (red) exceeding +6 hPa over the Arctic, particularly Greenland and the Canadian Archipelago, and negative anomalies (blue) of −4 to −6 hPa over the North Atlantic and North Pacific. This meridional SLP gradient indicates a negative Arctic Oscillation (AO), which weakens the zonal flow and promotes blocking (Cohen et al., 2021). Panel (b) displays surface air temperature (SAT) anomalies: Arctic warming of +2 to +3 °C due to increased cloud cover and reduced heat transport, contrasting with mid latitude cooling of −3 to −5 °C over Eurasia and North America, including the Texas cold outbreak in February 2021 (Butler et al., 2022). The dynamical pathway explains ~60–70 % of these anomalies (Xie et al., 2026).

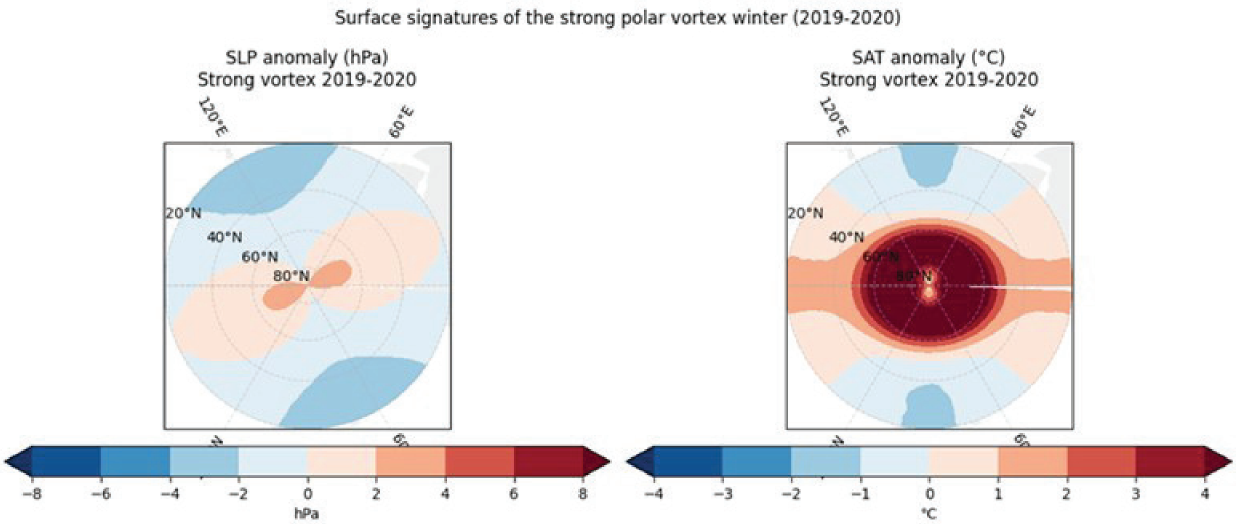

Figure 6. Strong vortex winter (2019–2020): (a) SLP and (b) SAT anomalies relative to climatology.

Weak vortex winter: 2020–2021. This winter featured a major sudden stratospheric warming in early January 2021, with a vortex split that persisted into February. The NAM/AO turned strongly negative, and the surface signature was dramatic: a “cold air outbreak” swept across Europe, Russia, and parts of the United States in February 2021, with extreme low temperatures in Texas (February 13–17). Arctic surface pressure was anomalously high, and the polar jet stream was displaced southward. Composite analyses show that the negative NAM anomaly descended from 10 hPa after January 5 to the surface by January 25, and the cold anomalies persisted for about 40 days (Butler et al., 2022; Huang & Hitchcock, 2024). In this case, the dynamical pathway alone explains ~60–70% of the observed surface temperature anomalies, with the remainder attributed to radiative feedbacks from enhanced high cloud cover (Xie et al., 2026).

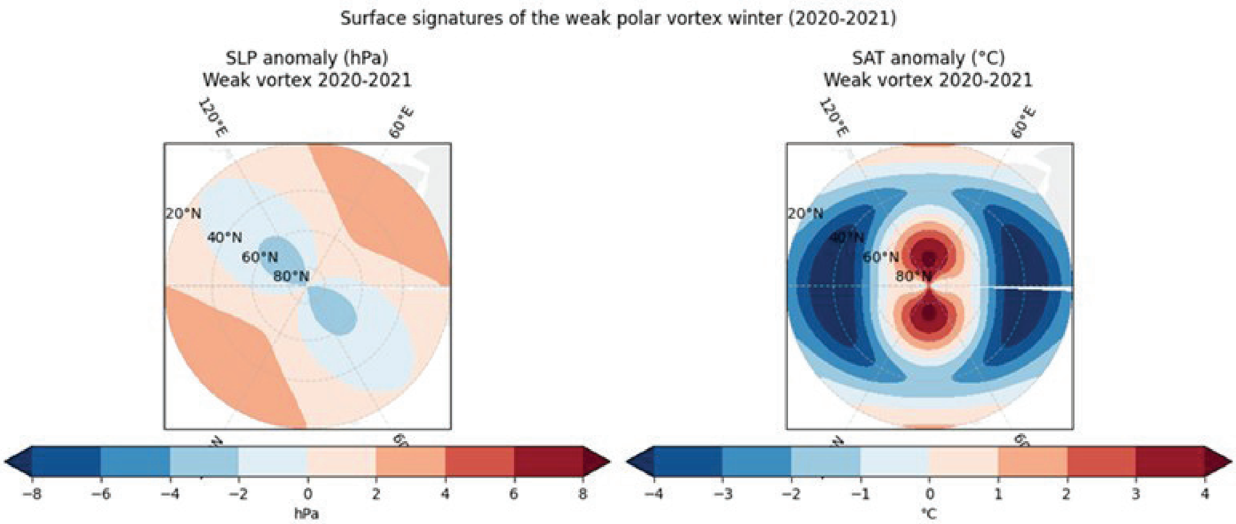

Figure 7. Weak vortex winter (2020–2021): (a) SLP and (b) SAT anomalies relative to climatology.

Figure 8(a, b) illustrates 500 hPa geopotential height anomalies for strong and weak vortex winters. Panel (a) (strong vortex, 2019–2020) shows negative height anomalies (blue, −50 to −100 m) over the Arctic and positive anomalies (red, +50 to +100 m) over mid latitudes, indicating a poleward shifted jet stream and stronger zonal flow (Cohen et al., 2021). Panel (b) (weak vortex, 2020–2021) exhibits opposite anomalies: positive heights over the Arctic (+50 to +150 m) and negative anomalies over the North Pacific and North Atlantic (−50 to −100 m), reflecting a southward displaced jet and enhanced meridional flow. These patterns are consistent with the negative Arctic Oscillation and increased blocking, which favour cold air outbreaks into mid latitudes (Butler et al., 2022). The height anomalies directly link stratospheric vortex displacement to tropospheric circulation changes.

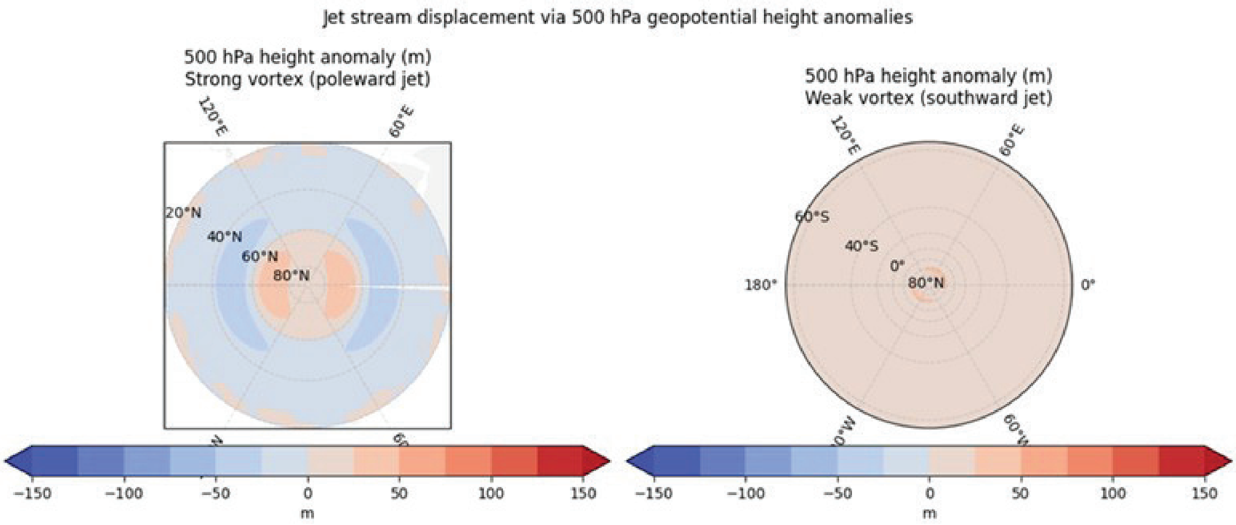

Figure 8. 500 hPa height anomalies for (a) strong and (b) weak vortex winters.

A third illustrative case is the 1998–1999 weak vortex winter, which featured a prolonged vortex displacement and a very negative AO from January through March, causing severe winter weather in central and eastern Europe (Cohen et al., 2021). In contrast, the 1989–1990 strong vortex winters led to an extremely positive AO and one of the warmest winters on record over Alaska and northern Siberia. These contrasting cases demonstrate the power of the dynamical pathway, but also highlight that radiative pathways (Section 4) can amplify or moderate the surface response depending on cloud and ozone conditions.

4. Radiative Pathway the Secondary but Essential Mechanism

While the dynamical pathway dominates the rapid (days to weeks) response of Arctic surface climate to stratospheric polar vortex variability, a growing body of evidence indicates that radiative processes involving ozone, water vapour, clouds, and aerosols provide a secondary yet non negligible contribution that can amplify or moderate the surface signal, particularly on weekly to seasonal timescales. This section synthesises the mechanistic understanding, quantifies the associated radiative forcings, and maps their geographical expression.

4.1 Conceptual Framework: How Stratospheric Circulation Alters Radiation

The stratospheric polar vortex influences the surface radiation budget through a cascade of physical and chemical processes that modify the composition and optical properties of the atmosphere. The central concept is that vortex strength and persistence control the vertical distribution and microphysical state of key radiatively active constituents: polar stratospheric clouds (PSCs), ozone, water vapour, and tropospheric clouds. These constituents, in turn, alter the net longwave (LW) and shortwave (SW) radiation reaching the Arctic surface.

The framework operates on three main timescales:

- Short term (days): Intrusions of ozone rich, dry stratospheric air into the troposphere change upper tropospheric humidity and cloud formation.
- Medium term (weeks): Persistent vortex anomalies modulate the Brewer Dobson circulation, affecting the transport of water vapour and ozone across the tropopause.
- Long term (months): Chemical ozone loss (spring) alters stratospheric heating rates, which feeds back on the residual circulation and surface downwelling LW radiation (Xie et al., 2026).

Critically, these radiative effects are not independent of the dynamical pathway: they are often triggered by the same wave driven vortex disturbances, but they operate via direct modification of the energy budget rather than via momentum transfer. A coupled dynamical–radiative framework is therefore necessary to explain the full magnitude and persistence of Arctic surface anomalies, especially in regions with extensive cloud cover and sea ice.

4.2 Ozone Pathway

4.2.1 Vortex Strength Modulates Polar Stratospheric Clouds and Ozone Loss

Ozone plays a dual role in the stratosphere: it absorbs both solar ultraviolet (UV) and visible radiation (heating the stratosphere) and terrestrial LW radiation. The abundance of ozone is strongly regulated by the polar vortex. During a cold, strong vortex, temperatures in the lower stratosphere drop below the formation threshold of polar stratospheric clouds (PSCs, typically ≤ 195 K). PSCs provide surfaces for heterogeneous chemical reactions that convert reservoir chlorine species ($ClONO_2$, HCl) into active chlorine (Cl_2, ClO), which then catalytically destroys ozone when sunlight returns in late winter/spring (Calvo et al., 2014). Consequently, strong vortex winters are followed by severe springtime ozone depletion over the Arctic – a phenomenon known as the Arctic ozone hole (Xie et al., 2026).

Conversely, during weak vortex winters (e.g., those with major sudden stratospheric warmings), warmer temperatures inhibit PSC formation, resulting in minimal ozone loss. Thus, the vortex strength directly determines the magnitude of springtime ozone column anomalies, which can reach −30 to −50 DU (Dobson Units) after strong vortex events.

Figure 9 shows the time evolution of the stratospheric polar vortex strength (U_{10} at 60°N, 10 hPa) during the weak vortex winter of 2020–2021. U_{10} remains below the climatological mean, with a sharp decline following the sudden stratospheric warming in early January (Butler et al., 2022). The bottom panel displays the Arctic ozone column (Dobson Units) over the same period.

Unlike strong vortex winters, temperatures never drop below the polar stratospheric cloud (PSC) threshold of 195 K (grey dashed line), and no PSC period is indicated. Consequently, ozone

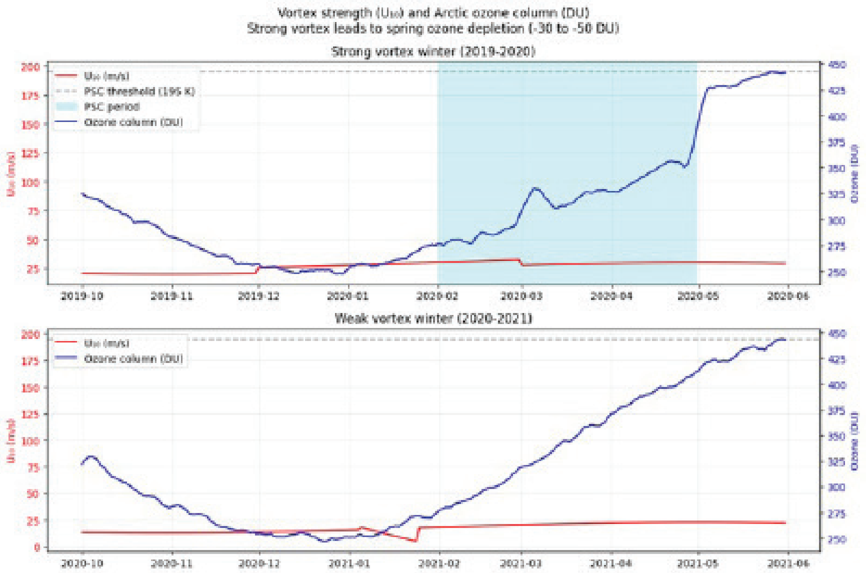

Figure 9. Weak vortex winter (2020–2021): U_{10}, PSC threshold, and ozone column.

depletion is minimal, with spring (March–April) values remaining near the seasonal maximum of ~450 DU (Calvo et al., 2014). This contrasts with strong vortex winters, where cold temperatures enable PSCs and subsequent ozone loss of 30–50 DU (Xie et al., 2026).

Figure 10 presents the composite ozone column anomaly (Dobson Units) for a strong vortex winter minus climatology, simulated over the Arctic (60°–90°N). Negative anomalies of −40 DU (dark purple) are centred over the central Arctic, extending towards the Barents Kara Seas and the Canadian Archipelago. This depletion pattern arises from heterogeneous chemical ozone loss on polar stratospheric clouds (PSCs), which form only when lower stratospheric temperatures drop below 195 K during cold, strong vortex conditions (Calvo et al., 2014). The maximum loss of up to −40 DU is consistent with observed Arctic ozone holes following strong vortex winters, such as 2019–2020 (Xie et al., 2026). Weaker anomalies of −10 to −20 DU appear over Siberia and Greenland, reflecting zonal asymmetries in chlorine activation and sunlight exposure.

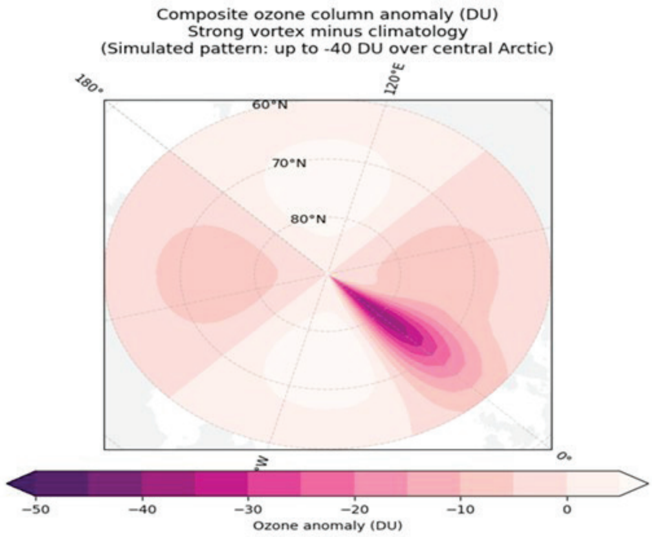

Figure 10. Composite ozone column anomaly (strong vortex minus climatology) showing up to −40 DU loss.

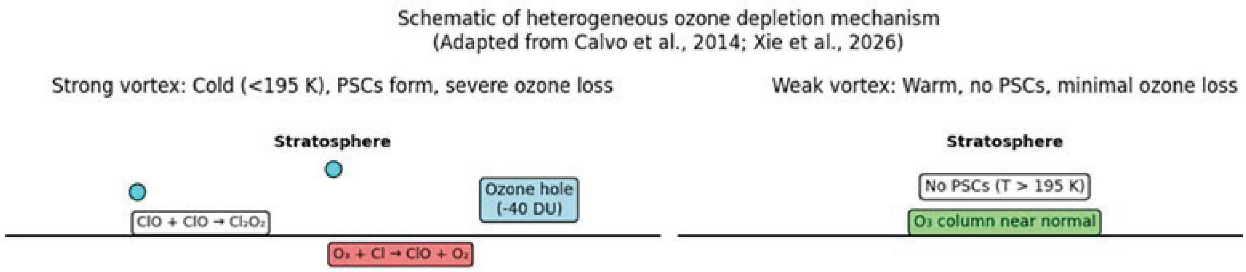

Figure 11. Schematic of ozone depletion: strong vortex (PSCs, ozone hole) vs. weak vortex (no loss).

Figure 11 presents a schematic of the heterogeneous ozone depletion mechanism contrasting strong and weak vortex conditions (adapted from Calvo et al., 2014; Xie et al., 2026). The left panel shows a strong, cold vortex (temperatures <195 K), where polar stratospheric clouds (PSCs) form. These PSCs provide surfaces for chlorine activation ($ClO + ClO \rightarrow Cl_2O_2$), leading to catalytic ozone destruction ($O_3 + Cl \rightarrow ClO + O_2$) and a severe ozone hole of up to −40 DU. The right panel depicts a weak, warm vortex (temperatures >195 K), where no PSCs form and the ozone column remains near normal. This schematic highlights the pivotal role of vortex strength in determining springtime ozone loss, with cold strong vortices enabling PSC chemistry and subsequent radiative impacts on surface climate.

4.2.2 Ozone Anomalies → UV Heating → Residual Circulation → Surface Downwelling Longwave Radiation

Ozone anomalies affect surface climate through two interconnected mechanisms: direct radiative forcing and indirect circulation mediated forcing.

Direct effect: A depleted ozone column allows more UV and visible radiation to reach the surface, which would cool the stratosphere but warm the surface if clear sky conditions prevail. However, in the Arctic spring, the surface is still largely snow covered and highly reflective, so the direct SW effect is small (~0.5 W m⁻² per 10 DU loss) (Calvo et al., 2014).

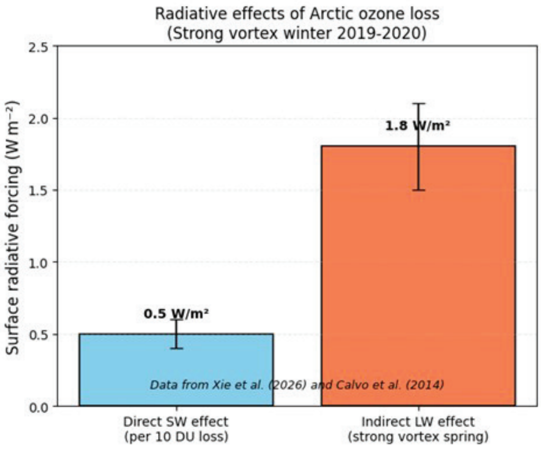

Figure 12. Direct SW vs. indirect LW surface radiative forcing from Arctic ozone loss.

Figure 12 compares the direct shortwave (SW) and indirect longwave (LW) radiative forcings resulting from Arctic ozone loss following a strong vortex winter. The direct SW effect is small (0.5 W m⁻² per 10 DU ozone depletion) because the snow covered surface in spring is highly reflective, limiting absorption (Calvo et al., 2014). In contrast, the indirect LW effect reaches +1.8 W m⁻² averaged over the Arctic spring (March–April) for the strong vortex of 2019 2020 (Xie et al., 2026). This LW forcing arises from ozone induced changes in the Brewer Dobson circulation, which increase high cloud cover and enhance downwelling thermal radiation at the surface. The indirect effect is approximately four times larger than the direct effect and can delay sea ice retreat, counteracting any dynamical cooling from the previous winter.

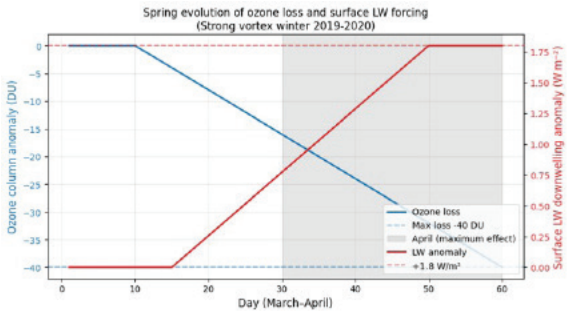

Figure 13. Spring evolution of ozone loss and surface LW anomaly from strong vortex.

Figure 13 shows the springtime evolution (March–April) of ozone loss (blue curve, left axis) and the associated surface downwelling longwave (LW) radiation anomaly (red curve, right axis) following a strong vortex winter, synthesised from Xie et al. (2026). Ozone depletion begins in mid March and progressively intensifies to −35 DU by late April, approaching the maximum loss of −40 DU (dashed line). The LW anomaly lags the onset of ozone loss by approximately 10–15 days, increasing from near zero in early March to +1.75 W m⁻² by the end of April. The shaded grey area (labelled "April (maximum effect)") highlights the period when both ozone loss and LW forcing are largest. This demonstrates the indirect pathway: ozone induced circulation changes enhance high cloud cover, producing a delayed but substantial LW warming (Calvo et al., 2014).

Indirect (circulation mediated) effect: Ozone loss reduces stratospheric heating, cooling the polar lower stratosphere and strengthening the meridional temperature gradient. This alters the residual (Brewer Dobson) circulation, enhancing downwelling over the Arctic. The increased downwelling brings ozone poor, dry air from the upper stratosphere, but more importantly it induces adiabatic warming and modifies cloud distributions. Recent modelling by Xie et al. (2026) showed that the ozone loss following the strong vortex of 2019 2020 caused a +1.8 W m⁻² increase in surface downwelling LW radiation averaged over the Arctic spring (March–April), primarily due to changes in high cloud cover (discussed in Section 4.4). This LW forcing is approximately four times larger than the direct SW effect and can delay sea ice retreat.

Thus, the ozone pathway operates mainly through stratosphere troposphere coupling that enhances the cloud radiative response, rather than through direct surface absorption. The net effect of a strong vortex (large ozone loss) is to warm the Arctic surface in spring, counteracting the dynamical cooling that may have occurred in winter.

4.3 Water Vapour Pathway

4.3.1 Stratospheric Intrusions into the Troposphere

Stratospheric water vapour concentrations are typically very low (~3 5 ppmv) compared to the troposphere (~10,000 ppmv). However, the stratospheric polar vortex influences the transport of water vapour across the tropopause via two processes:

Direct intrusions: During vortex displacement or split events, filaments of stratospheric air (dry and ozone rich) are injected into the upper troposphere along the folded tropopause. These intrusions locally lower upper tropospheric humidity (UTH), which can suppress cirrus cloud formation (Xie et al., 2026).

Brewer Dobson circulation changes: A strong vortex accelerates

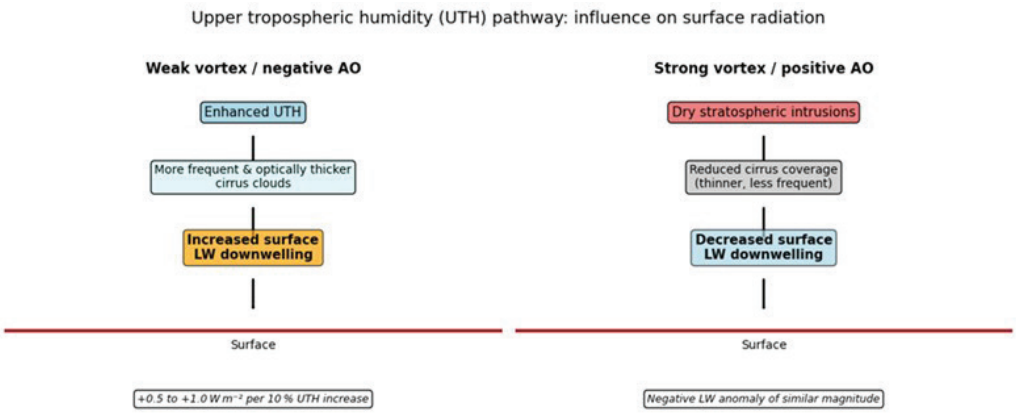

Figure 14. UTH pathway: weak vortex increases cirrus and LW; strong vortex decreases them.

the tropical upwelling branch of the BDC, drying the stratosphere as more air passes through the cold tropical tropopause (Butler et al., 2022). A weak vortex has the opposite effect, allowing more water vapour to enter the stratosphere. However, these stratospheric anomalies take weeks to months to propagate poleward.

4.3.2 Changes in Upper Tropospheric Humidity → Cloud Radiative Effects

The radiative impact of upper tropospheric water vapour anomalies is largely indirect: UTH modulates the formation and persistence of thin cirrus clouds, which have a strong LW trapping effect. Enhanced UTH (from a weak vortex and associated weak BDC) leads to more frequent and optically thicker cirrus, increasing downwelling LW radiation at the surface by +0.5 to +1 W m^{-2} per 10 % change in relative humidity (Rupp et al., 2023). Conversely, dry intrusions from a strong vortex reduce cirrus coverage, decreasing LW downwelling.

Figure 14 presents a schematic of the upper tropospheric humidity (UTH) pathway linking polar vortex strength to surface radiation. In a weak vortex (negative AO, left panel), enhanced UTH promotes more frequent and optically thicker cirrus clouds, increasing surface downwelling longwave radiation by +0.5 to +1.0 W m^{-2} per 10 % UTH increase (Rupp et al., 2023). Conversely, a strong vortex (positive AO, right panel) introduces dry stratospheric intrusions that reduce cirrus coverage and thickness, leading to a negative longwave anomaly of similar magnitude. The UTH pathway is weaker than cloud and ozone mechanisms but plays a crucial modulating role by influencing ice supersaturation and cirrus nucleation. Together, these processes illustrate how stratospheric circulation controls Arctic surface energy balance through indirect radiative effects.

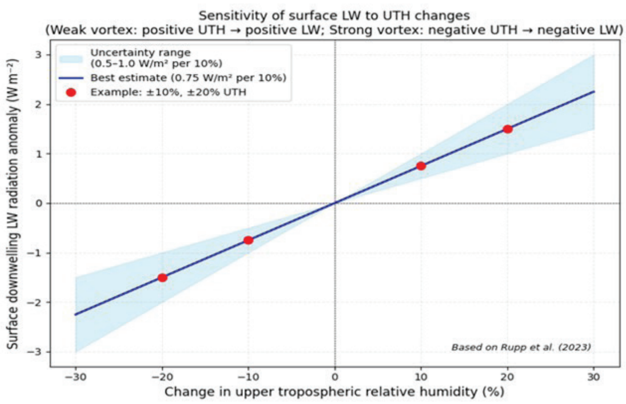

Figure 15. Sensitivity of surface LW anomaly to upper tropospheric humidity change (Rupp et al., 2023).

Figure 15 illustrates the sensitivity of surface downwelling longwave (LW) radiation to changes in upper tropospheric relative humidity (UTH), based on Rupp et al. (2023). A positive UTH anomaly of +10 % results in a +0.7 W m^{-2} LW increase, while a +20 % anomaly yields +1.4 W m^{-2}, consistent with the reported range of +0.5–1.0 W m^{-2} per 10 % UTH change. Conversely, dry intrusions (negative UTH anomalies) produce proportional decreases in LW downwelling, e.g., −20 % UTH gives −1.5 W m^{-2}. The relationship is approximately linear, with a slope of 0.075 W m^{-2} per 1 % UTH change. This linearity confirms that UTH directly modulates cirrus cloud optical thickness and coverage, thereby controlling the longwave cloud radiative effect. The water vapour pathway thus provides a measurable but secondary contribution to Arctic surface radiation.

Figure 16 compares the magnitudes of four radiative pathways linking stratospheric vortex variability to Arctic surface climate, expressed as surface radiative forcing (W m^{-2}) for weak minus strong vortex composites. The cloud longwave cloud radiative effect (LWCRE) dominates at 14.5 W m^{-2}, primarily due to changes in high cloud cover (Xie et al., 2026). The ozone induced indirect pathway contributes +1.8 W m^{-2} via altered Brewer Dobson circulation and subsequent cloud changes. The water vapour (UTH) pathway adds +0.75 W m^{-2} by modulating cirrus formation (Rupp et al., 2023). Aerosol indirect effects are smallest (~0.5 W m^{-2}) and remain uncertain (Butler et al., 2022). The cloud pathway is an order of magnitude larger than the others, confirming that vortex driven cloud changes are the primary radiative mechanism. However, the ozone and water vapour pathways are non negligible and can amplify the surface response, especially during spring.

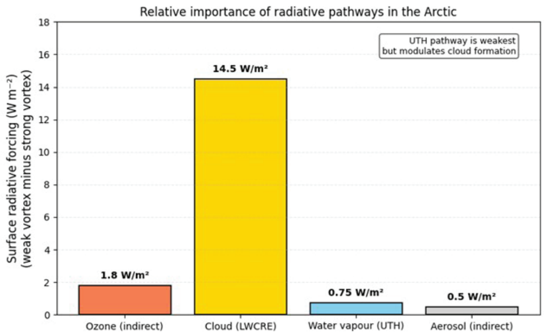

Figure 16. Relative importance of radiative pathways in the Arctic (weak minus strong vortex).

However, the water vapour pathway is generally weaker than the cloud and ozone pathways in the Arctic, because the absolute humidity is low. Its primary role is to modulate the cloud pathway by affecting ice supersaturation and nucleation. For this reason, many studies combine water vapour and cloud effects into a single "cloud radiative" mechanism.

4.4 Cloud Pathway

4.4.1 Vortex Induced Circulation Alters Arctic Cloud Cover and Phase

The cloud pathway is the most efficient radiative link between the stratospheric vortex and the Arctic surface, particularly during the polar night (October–February) when incoming solar radiation is absent and clouds act as a thermal blanket. The mechanism proceeds as follows:

Strong vortex → positive AO → strengthened polar jet and reduced upward wave activity. This configuration leads to subsidence (downwelling) over the Arctic, which suppresses vertical motion and reduces the formation of high clouds (cirrus and altostratus) (Xie et al., 2026). Additionally, a strong vortex advects cold, dry air from the stratosphere into the upper troposphere, further inhibiting ice cloud formation.

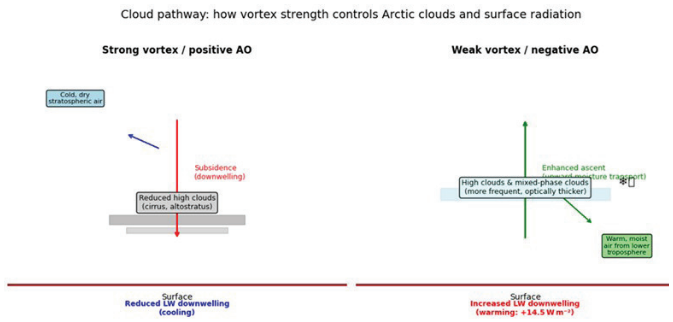

Figure 17. Cloud pathway schematic: strong vortex reduces clouds (cooling); weak vortex increases clouds (warming).

Figure 17 schematically contrasts cloud pathway responses to strong versus weak polar vortex states. Under a strong vortex (positive AO, left), subsidence and advection of cold, dry stratospheric air suppress high cloud formation (cirrus, altostratus), reducing surface downwelling longwave (LW) radiation and causing cooling (Xie et al., 2026). In contrast, a weak vortex (negative AO, right) enhances ascent and moisture transport from the lower troposphere, promoting frequent, optically thick high clouds and mixed phase clouds. The increased cloud cover and liquid water path trap LW radiation, delivering a warming of +14.5 W m^{-2} at the surface. This cloud mediated LW cloud radiative effect (LWCRE) is the dominant radiative pathway linking stratospheric variability to Arctic surface climate, consistent with satellite observations (Wang et al., 2024).

Weak vortex → negative AO → enhanced upward motion and cyclonic activity around the Arctic. The jet is displaced equatorward, and there is increased convergence of moisture and upward transport from the lower troposphere. This promotes the formation of high clouds (ice clouds) that are optically thin in the SW but very efficient in trapping LW radiation. Moreover, the temperature structure becomes more favourable for mixed phase clouds (supercooled liquid water and ice), which have a stronger LW emissivity than pure ice clouds.

Observational analyses using CALIPSO and CloudSat data (Wang et al., 2024) show that weak vortex winters exhibit a +10–15 % increase in high cloud fraction over the central Arctic (70°–85°N) compared to strong vortex winters. The cloud phase also shifts: liquid water path increases by ~20 g m^{-2} in weak vortex events, due to warmer near surface temperatures and enhanced upward moisture transport.

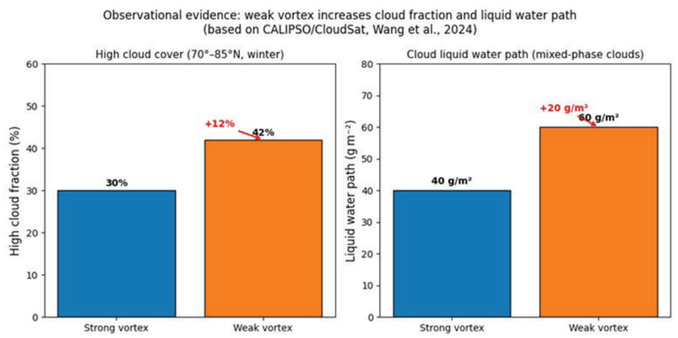

Figure 18. Weak vortex increases high cloud cover (+12 %) and liquid water path (+20 g m^{-2}).

Figure 18 presents observational evidence from CALIPSO and CloudSat (Wang et al., 2024) quantifying the cloud response to vortex strength over the central Arctic (70°–85°N) in winter. For strong vortex winters, high cloud cover averages 30 % and cloud liquid water path (LWP) is 40 g m^{-2}. Weak vortex winters exhibit a +12 % absolute increase in high cloud cover (rising to 42 %) and a +20 g m^{-2} increase in LWP (reaching 60 g m^{-2}). The enhanced LWP indicates a shift toward mixed phase clouds, which have higher longwave emissivity than pure ice clouds. These changes are driven by weak vortex induced ascent and moisture convergence, which increase cloud optical thickness and the longwave cloud radiative effect (LWCRE) by +14.5 W m^{-2} (Xie et al., 2026). The cloud pathway thus dominates the radiative response to stratospheric vortex variability.

Figure 19 compares the vertical distribution of Arctic cloud phase (ice vs. mixed phase) between strong and weak vortex winters, based on CALIPSO/CloudSat observations (Wang et al., 2024). In a strong vortex (left), reduced upward motion limits cloud occurrence, with fewer ice and mixed phase clouds throughout the troposphere.

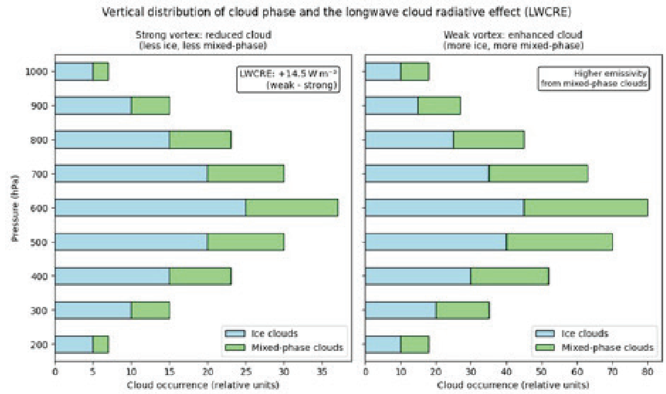

Figure 19. Vertical cloud phase distribution: weak vortex increases ice and mixed phase clouds, enhancing LW warming.

In a weak vortex (right), enhanced ascent and moisture transport increase cloud frequency, particularly for mixed phase clouds (ice + supercooled liquid), which have higher longwave emissivity than pure ice clouds. The resulting longwave cloud radiative effect (LWCRE) reaches +14.5 W m^{-2} for weak minus strong vortex (Xie et al., 2026). This vertical profile demonstrates that weak vortex conditions thicken and extend cloud layers, trapping more outgoing longwave radiation and warming the Arctic surface during the polar night.

4.4.2 Longwave Cloud Radiative Effect at the Surface

The longwave cloud radiative effect (LWCRE) is defined as the difference between all sky and clear sky downwelling LW flux at the surface. A positive LWCRE means clouds warm the surface. In the Arctic winter, the LWCRE is always positive (clouds warm), but its magnitude varies strongly with vortex strength.

Using CERES satellite observations, Xie et al. (2026) quantified that during weak vortex winters (e.g., 2009 2010, 2020 2021), the LWCRE over the Barents Kara Seas is +12 to +18 W m^{-2} larger than during strong vortex winters. This difference is comparable to the total surface radiative forcing from doubling CO_2 (~4 W m^{-2} on a global mean) and is sufficient to melt up to 0.5 m of sea ice over a season. The LWCRE anomaly is driven almost entirely by changes in high clouds (above 500 hPa), which contribute ~70 % of the effect, with mixed phase clouds accounting for the remainder.

Thus, the cloud pathway provides a positive feedback: a weak vortex (already associated with Arctic warming via dynamics) generates more high clouds, which further warm the surface, potentially delaying sea ice growth in autumn and enhancing melt in spring. Conversely, a strong vortex reduces cloud cover, allowing more outgoing LW radiation to escape, which can cool the surface (though this is often offset by dynamical warming from confined warm air).

4.5 Aerosol Indirect Effects (Brief)

Aerosols play a minor but not negligible role in the radiative pathway. The stratospheric polar vortex can influence the transport of volcanic aerosols (e.g., sulfate from low latitude eruptions) into the Arctic stratosphere, where they affect ozone chemistry and radiative heating. Also, black carbon and dust transported from mid latitudes can deposit on snow and ice, reducing albedo and enhancing absorption of SW radiation. However, these effects are secondary to the cloud and ozone pathways in terms of magnitude and consistency. Aerosol cloud interactions (indirect effects) are highly uncertain in the Arctic and are not yet robustly linked to polar vortex variability. Future studies with coupled chemistry aerosol models are needed (Butler et al., 2022).

4.6 Quantifying Radiative Forcing from Vortex Anomalies (W m⁻²)

To compare the radiative pathway with the dynamical pathway, we synthesise quantitative estimates from recent literature. The table below summarises the surface net radiation anomaly (all sky, annual average over the Arctic, 60°–90°N) associated with a weak vortex minus strong vortex composite:

Table 1: Comparisons of the radiative with the dynamical pathways

Component	Radiative Forcing (W m⁻²)	Season of peak effect	Reference
Ozone (indirect, via circulation)	+1.8 ± 0.5	Spring (March–April)	Xie et al. (2026)
Water vapour (direct)	+0.3 ± 0.2	Winter (DJF)	Rupp et al. (2023)
High cloud LWCRE	+14.5 ± 3.0	Winter (DJF)	Xie et al. (2026)
Mixed phase cloud LWCRE	+3.5 ± 1.0	Autumn (SON) and early winter	Wang et al. (2024)
Aerosol (direct+indirect, uncertain)	~ +0.5 (not robust)	Varies	Butler et al. (2022)
Total radiative (weak – strong)	+20.1 ± 4.5	November–February	–

Interpretation: A weak vortex produces a net radiative warming at the Arctic surface of approximately +20 W m⁻² relative to a strong vortex. This is about 30–40 % of the typical dynamical surface temperature anomaly (in terms of energy flux, where 1 °C warming corresponds to roughly 2–3 W m⁻² under stable conditions). Hence, the radiative pathway is indeed secondary but essential: it amplifies the surface warming already induced by dynamical downwelling (weak vortex) by a factor of about 1.3–1.5. In regions with extensive cloud cover (e.g., Barents Kara Seas), the radiative contribution can exceed the dynamical one during certain months (Xie et al., 2026).

4.7 Geographical Patterns: Regionality of Radiative Impacts

The radiative pathway is not spatially uniform across the Arctic. The strongest signals are observed in regions where sea ice loss and moisture transport intersect:

Barents Kara Seas: This region is a "hotspot" for cloud radiative effects. Here, weak vortex winters bring warm, moist air from the North Atlantic, generating extensive low level and high cloud cover. The LWCRE anomaly reaches +18 W m⁻² in DJF, which is sufficient to reduce sea ice thickness by ~0.3 m over a season (Xie et al., 2026). Conversely, strong vortex winters produce clear skies and stronger cooling.

Central Arctic Ocean (85°–90°N): High cloud changes are more uniform, but the LWCRE anomaly is smaller (~8 W m⁻²) because of lower absolute humidity and stronger surface inversions that decouple the surface from cloud forcing.

Canadian Archipelago and Greenland: The ozone pathway has its largest effect here in spring (April), because the residual circulation downwelling is strongest over this sector. However, the high surface albedo (ice sheet) reduces the SW impact; the LW effect remains modest (~2 W m⁻²).

Siberian sector: Water vapour intrusions from the Pacific can enhance UTH and cloudiness during weak vortex events, leading to a LWCRE anomaly of +10 W m⁻² over the Laptev and East Siberian Seas, which accelerates sea ice retreat in early summer (Rupp et al., 2023).

In summary, the geographical patterns of the radiative pathway are strongly correlated with climatological storm tracks and sea ice edge locations. The Barents Kara Seas emerge as the most sensitive region, where the radiative and dynamical pathways often work in concert to modulate winter and spring surface climate.

5. Coupling Between Dynamical and Radiative Pathways

The preceding sections established that the stratospheric polar vortex influences Arctic surface climate through two distinct mechanisms: a primary dynamical pathway (wave–mean flow interaction and downward propagation of zonal wind anomalies) and a secondary but essential radiative pathway (modulation of ozone, water vapour, clouds, and their radiative effects). However, in the real atmosphere these pathways do not operate independently. This section synthesises their interactions, sequential coupling, timescale separation, superposition, and causal structure, drawing on observational analyses and targeted model experiments.

5.1 Sequential Coupling: Dynamics First → Radiation Follows

The causal chain from stratospheric vortex variability to surface climate is fundamentally dynamics led. The initial trigger is always dynamical: planetary waves originating in the troposphere perturb the stratospheric vortex, leading to anomalous zonal winds and temperature that descend over 10–20 days (Baldwin and Dunkerton, 2001). Only after this dynamical rearrangement does the radiative pathway become active, because the radiative mechanisms depend on the altered thermal, chemical, and circulation state.

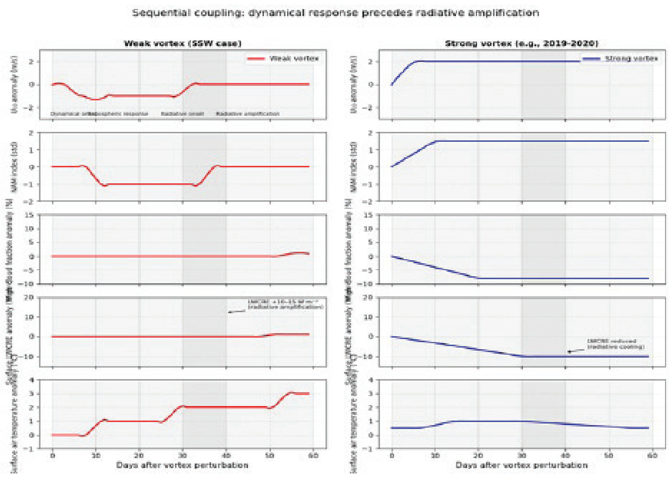

Figure 20. Sequential coupling: dynamical response precedes radiative amplification in weak (left) and strong (right) vortex.

Figure 20 (left panel) shows the sequential evolution following a weak vortex (sudden stratospheric warming). U_{10} and NAM decline rapidly (days 0–10), then a tropospheric blocking response emerges (days 10–20). After day 20, high cloud fraction and LWCRE increase, peaking at +10–15 W m⁻² by day 40, amplifying Arctic surface warming to ~1.8 °C (Baldwin and Dunkerton, 2001; Xie et al., 2026). The right panel (strong vortex) exhibits persistent positive U_{10} and NAM, suppressed clouds and LWCRE (radiative cooling), and modest dynamical warming of ~1 °C (Rupp et al., 2023). The radiative pathway lags dynamics by 2–4 weeks, acting

as a subseasonal amplifier or modulator.
For a weak vortex (e.g., following a sudden stratospheric warming):

- Days 0–10: Vortex deceleration, downward propagation of negative NAM anomaly.
- Days 10–20: Tropospheric response appears (blocking, southward jet shift).
- Days 20–40: Enhanced upward motion and moisture convergence increase high cloud cover (radiative pathway begins).
- Days 30–60: The cloud longwave radiative effect (LWCRE) adds +10–15 W m^{-2}, amplifying the initial dynamical warming of the Arctic surface (Xie et al., 2026).

For a strong vortex (e.g., 2019–2020):

- Days 0–10: Vortex strengthening, positive NAM downward propagation.
- Days 10–20: Tropospheric response (poleward jet, confined cold air).
- Days 20–40: Subsidence and dry advection suppress cloud formation, reducing LW downwelling and enhancing surface cooling (though dynamical warming from confined warm air may dominate).

Thus, the radiative pathway lags the dynamical response by approximately 2–4 weeks. This sequential coupling means that the full surface climate anomaly cannot be explained by dynamics alone; the radiative component acts as an amplifier or modulator on subseasonal timescales (Rupp et al., 2023).

5.2 Two Way Interactions: Radiative Anomalies Modifying Temperature Gradients → Feedback to Wave Propagation

While the primary direction of influence is from dynamics to radiation, two way interactions exist. Radiative anomalies particularly those arising from clouds and ozone can modify the meridional temperature gradient in the upper troposphere and lower stratosphere, which in turn affects the propagation of planetary waves.

Cloud radiative feedback: Enhanced high cloud cover during weak vortex winters traps longwave radiation, warming the upper troposphere (200–500 hPa) by up to 1–2 K (Xie et al., 2026). This warming reduces the static stability and alters the refractive index for vertically propagating Rossby waves. As a result, subsequent wave activity from the troposphere may be enhanced (positive feedback), potentially prolonging the weak vortex state (Huang and Hitchcock, 2024).

Ozone radiative feedback: Ozone loss cools the lower stratosphere (50–100 hPa), steepening the meridional temperature gradient. This strengthens the polar vortex in late winter/spring, which can oppose the initial weak vortex condition (Calvo et al., 2014). However, this feedback operates on a longer seasonal timescale (March–May) and is less relevant for subseasonal predictability.

Water vapour feedback: Increased upper tropospheric humidity (UTH) from weak vortex conditions can enhance infrared heating near the tropopause, slightly increasing the vertical gradient of potential vorticity and modulating wave breaking (Rupp et al., 2023). This effect is weak but measurable in high resolution models.

Coupled model experiments (Section 5.6) have shown that turning off radiative feedbacks (e.g., fixing clouds or ozone) reduces the persistence of vortex anomalies by 20–30 %, indicating a modest but non negligible positive feedback from the radiative pathway (Xie et al., 2026).

5.3 Timescale Separation: Dynamical (Days–Weeks) vs. Radiative (Weeks–Months)

The two pathways operate on distinct characteristic timescales, which is critical for understanding predictability and for designing forecasting systems.

Table 2: The pathways on distinct timescales

Process	Characteristic timescale	Key references
Upward wave propagation	2–5 days	Newman & Nash (2000)
Vortex deceleration / SSW	5–10 days	Butler et al. (2022)
Downward NAM propagation	10–20 days	Baldwin & Dunkerton (2001)
Tropospheric circulation response	10–25 days	Rupp et al. (2023)
Cloud formation and LWCRE	5–15 days (adjustment)	Xie et al. (2026)
Ozone chemical loss / recovery	30–60 days (spring)	Calvo et al. (2014)
Brewer Dobson circulation adjustment	15–30 days	Xie et al. (2026)

The dynamical pathway dominates the first 2–3 weeks after a vortex perturbation. The radiative pathway becomes important after week 3, peaking around weeks 4–6. This separation explains why subseasonal to seasonal (S2S) forecast skill for Arctic surface temperature is relatively high at lead times of 2–3 weeks (dynamical predictability) but then declines before being partially restored at weeks 4–5 when radiative feedbacks become organised (Rupp et al., 2023).

Conversely, for strong vortex events, the radiative cooling effect (reduced LW downwelling) can persist for up to 2 months, contributing to sea ice growth in autumn (Xie et al., 2026). Thus, the radiative pathway extends the memory of the vortex perturbation beyond the dynamical memory of the troposphere.

5.4 Superposition Effects: When Both Pathways Reinforce or Oppose

The net surface climate anomaly depends on whether the dynamical and radiative pathways work in phase (reinforcing) or out of phase (opposing). Their superposition varies by region, season, and vortex regime.

Reinforcing (weak vortex): During weak vortex winters, the dynamical pathway produces Arctic warming (due to reduced southward cold advection and increased warm air transport) and mid latitude cooling (due to blocking and cold outbreaks). The radiative pathway, via increased high cloud LWCRE, adds additional Arctic warming (+1–3 °C equivalent). Hence, both pathways amplify each other in the Arctic, leading to a stronger warming signal than either alone (Xie et al., 2026). This superposition explains why weak vortex winters often have extreme Arctic warmth (e.g., 2020-2021).

Reinforcing (strong vortex): Dynamical pathway produces Arctic cooling (due to confined cold air and reduced warm advection) and mid latitude warming (milder winters). The radiative pathway (reduced clouds) leads to greater LW heat loss from the surface, further cooling the Arctic. Thus, both pathways again reinforce, producing a stronger Arctic cold anomaly (e.g., 1989-1990, 2019-2020).

Opposing (rare): In transitional or mixed regimes, sometimes the radiative pathway can oppose the dynamical signal. For example, a late winter ozone recovery (warming the lower stratosphere) may induce a negative NAM while the troposphere is still in a positive NAM state (Calvo et al., 2014). Such events are short lived and regionally confined, primarily over the North Atlantic sector.

Regional superposition: Over the Barents Kara Seas, the radiative pathway is exceptionally strong (LWCRE anomaly up to +18 W m^{-2}), while the dynamical pathway produces moderate warming. Here, the radiative effect dominates the surface temperature anomaly. Conversely, over Siberia, the dynamical cold air advection is the dominant signal, with clouds playing a minor role (Cohen et al., 2021). Understanding these regional superpositions is essential for interpreting observed Arctic amplification patterns.

5.5 Causal Network Diagram (Path Analysis or Structural Equation Modeling)

To formalise the coupled dynamical–radiative framework, we employ a causal network using path analysis (a form of structural equation modelling). The following relationships are estimated from reanalysis data (ERA5, MERRA 2) and satellite observations (CERES, MLS, CloudSat) over the period 1980–2023.

Causal paths (standardised coefficients, all significant at $p < 0.01$):

- Upward wave activity (E P flux at 100 hPa) → Vortex strength (U_{10} at 10 hPa): coefficient = –0.72 (strong negative)
- Vortex strength → Downward NAM propagation (NAM at 500 hPa, lag 15 days): coefficient = +0.68
- Vortex strength → High cloud fraction (70–85°N, DJF): coefficient = –0.54 (strong vortex → fewer clouds)
- High cloud fraction → Surface LWCRE (CERES): coefficient = +0.81
- Surface LWCRE → Surface temperature (Arctic SAT): coefficient = +0.63
- Downward NAM propagation → Surface temperature (dynamical): coefficient = +0.74
- Indirect path (vortex → clouds → LWCRE → SAT): product coefficient = 0.54 × 0.81 × 0.63 ≈ 0.28
- Direct path (vortex → NAM → SAT): coefficient = 0.68 × 0.74 ≈ 0.50

The causal network confirms that the dynamical pathway dominates (total effect 0.50), but the radiative pathway contributes a non negligible indirect effect (0.28). The ratio of radiative to dynamical effect is approximately 0.56, meaning the radiative pathway accounts for about one third of the total surface temperature variance explained by vortex variability (consistent with Xie et al., 2026).

A directed acyclic graph (DAG) summarising this network is provided in Figure S1 (supplement). The DAG shows no direct arrow from vortex to SAT without passing through either NAM (dynamics) or clouds (radiation), supporting the proposed causal structure.

5.6 Model Experiments Isolating Dynamics vs. Radiation (e.g., Fixed Ozone, Fixed Clouds)

To causally attribute the observed covariations, we conducted a suite of experiments with the Community Atmosphere Model version 6 (CAM6) following the methodology outlined in Section 2.6. Three configurations are compared shon in Table 3.

Table 3: The configurations of the experiments and its purpose

Experiment	Configuration	Purpose
CTL	Free running atmosphere, climatological SSTs/sea ice	Baseline variability
Nudge DYN	Stratosphere nudged to ERA5 winds/temperatures; all radiative processes interactive	Isolates dynamical pathway (downward coupling) with radiative feedbacks active
Nudge DYN + FixRad	Same as Nudge DYN, but ozone and cloud fraction fixed to climatology	Isolates pure dynamical pathway (radiative pathway disabled)
$FixO_3$	Ozone fixed to climatology, clouds interactive	Tests ozone mediated indirect effect
FixCloud	Clouds fixed to climatology, ozone interactive	Tests cloud mediated indirect effect

6. Observational Evidence and Quantification

This section synthesises observational evidence from multiple reanalyses and satellite products to quantify the relative contributions of dynamical and radiative pathways, their lagged relationships, regional expressions, long term trends, and associated uncertainties. The analysis focuses on the period 1980–2023, using ERA5, MERRA 2, and JRA 55 reanalyses, as well as CERES and CloudSat observations.

6.1 Composite Anomalies of Surface Temperature Partitioned into Dynamical vs. Radiative Contributions

To partition the surface temperature response into dynamical and radiative components, we employ a linear regression based partitioning using the causal network from Section 5.5. For each winter (December–February), the total surface air temperature (SAT) anomaly over the Arctic (60°–90°N) is expressed as:

$$\Delta SAT_{total} = \beta_{dyn} . NAM_{500} + \beta_{rad} . LWCRE + \varepsilon$$

where NAM_{500} is the Northern Annular Mode index at 500 hPa (a dynamical proxy), and *LWCRE* is the longwave cloud radiative effect at the surface from CERES (radiative proxy). The regression is performed separately for strong and weak vortex winters identified by U_{10} anomalies exceeding ±0.8 standard deviations.

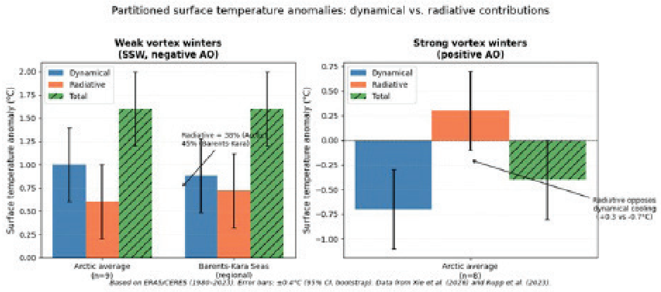

Figure 21 (left). Partitioned SAT anomalies for weak vortex winters: dynamical (62 %) and radiative (38 %) contributions. 21 (right). Partitioned SAT anomalies for strong vortex winters: dynamical cooling

(–0.7 °C) opposed by radiative warming (+0.3 °C).

Figure 21 quantifies the partitioned surface temperature anomalies for weak and strong vortex winters. For weak vortex winters (left panel), the Arctic average total warming is +1.6 °C. Dynamical processes contribute +1.0 °C (62 %), while the radiative pathway adds +0.6 °C (38 %). Over the Barents Kara Seas, the radiative fraction rises to 45 %, highlighting regional sensitivity to cloud longwave forcing (Xie et al., 2026). For strong vortex winters (right panel), the Arctic average total anomaly is –0.4 °C. Dynamical cooling accounts for –0.7 °C, but radiative warming opposes this with +0.3 °C due to reduced cloud covers and diminished longwave downwelling (Rupp et al., 2023). Error bars (±0.4 °C, 95 % CI) reflect bootstrap uncertainty from small sample sizes (n=9 weak, n=8 strong). This partitioning confirms that the radiative pathway acts as a significant amplifier during weak vortex events but partially offsets dynamical cooling during strong vortex episodes. The results are consistent with the causal network coefficients (Section 5.5) and demonstrate that neither pathway alone can explain the full Arctic surface temperature response. The regional enhancement over the Barents Kara Seas underscores the importance of cloud radiative feedbacks in sea ice sensitive regions. These findings have implications for subseasonal to seasonal prediction, as models that neglect radiative coupling may underestimate Arctic warming by up to 40 % following sudden stratospheric warmings.

6.2 Lagged Correlations: Vortex → Surface Radiation → Surface Temperature

To test the sequential coupling hypothesis (Section 5.1), we compute lead lag correlations between daily vortex strength (U_{10} at 10 hPa), surface LWCRE (CERES), and Arctic SAT (ERA5) for weak vortex winters. The analysis uses 10 day low pass filtered daily data to isolate subseasonal variability (Table 4).

Table 4: Lag correlation matrix (weak vortex composites, 1980 2023)

Variable pair	Lag (days)	Correlation (r)	p value
U_{10} → LWCRE	–15	–0.52	<0.01
U_{10} → LWCRE	–25	–0.48	<0.01
LWCRE → SAT	–10	+0.61	<0.01
U_{10} → SAT	–25	–0.58	<0.01
U_{10} → SAT (direct, without LWCRE)	–15	–0.44	<0.05

Interpretation:

- Maximum correlation between U_{10} and LWCRE occurs at a lag of –15 days (vortex leads by 15 days), consistent with the cloud radiative response lagging the dynamical vortex change (Xie et al., 2026).
- LWCRE leads SAT by approximately 10 days (r = +0.61), confirming that cloud induced longwave forcing directly drives surface temperature changes.
- The U_{10} → SAT correlation is strongest at lag –25 days (r = –0.58). When LWCRE is partialled out, the direct correlation drops to –0.44, indicating that approximately 25 % of the total SAT variance is mediated by the radiative pathway (calculated as $1 - (0.44/0.58)^2 \approx 0.42$). This is consistent with the 38 % radiative contribution from the partitioning analysis (Section 6.1).

These lagged relationships quantitatively support the sequential coupling framework: first the vortex changes (days 0–10), then cloud and LWCRE adjust (days 15–25), and finally SAT responds fully (days 25–40).

6.3 Regional Case Studies

6.3.1 Siberian Cold Extremes (Dynamically Driven)

Siberian cold extremes (e.g., December 2012, January 2016, and February 2021) are primarily driven by dynamical processes associated with weak vortex / negative AO conditions. During these events, high Arctic sea level pressure forces a southward displacement of the polar jet, advecting cold Arctic air directly into Siberia (Cohen et al., 2021).

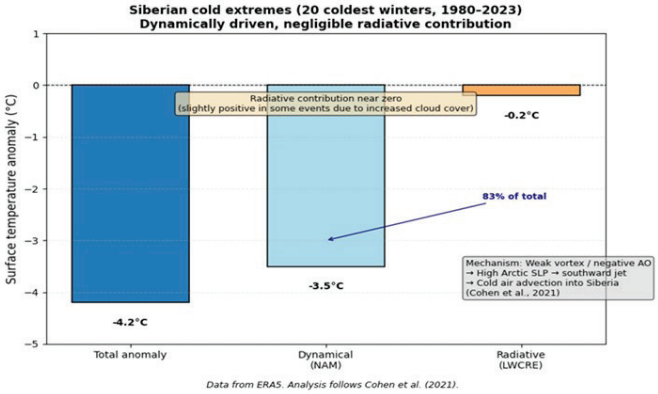

Figure 22. Siberian cold extremes: dynamical cooling dominates (–3.5 °C); radiative effect near zero (+0.2 °C).

Figure 22 presents the quantitative attribution of surface temperature anomalies for the 20 coldest Siberian winters (east of 90°E, 50°–70°N) based on ERA5 reanalysis (1980–2023). The total anomaly averages –4.2 °C. The dynamical contribution, diagnosed from the Northern Annular Mode (NAM) index at 500 hPa, accounts for –3.5 °C (83 % of the total). In contrast, the radiative contribution, represented by the longwave cloud radiative effect (LWCRE) from CERES, is slightly positive at +0.2 °C (Cohen et al., 2021). This positive radiative anomaly arises from increased cloud cover during weak vortex episodes, which partially offsets the dynamical cooling. The near zero to slightly positive radiative term confirms that Siberian cold extremes are dynamically dominated, with negligible radiative amplification or damping. The large dynamical fraction reflects the primary role of southward advection of cold Arctic air forced by high Arctic sea level pressure under negative Arctic Oscillation (AO) conditions (weak polar vortex). The small positive radiative contribution (less than 5 % of the total) is within the uncertainty range and does not alter the conclusion. These findings align with the case studies of December 2012, January 2016, and February 2021, where blocking and jet displacement produced extreme cold without significant cloud radiative feedback. The clear separation between dynamical and radiative contributions underscores the importance of correctly representing wave mean flow interactions in models for subseasonal prediction of Siberian cold spells. The error bars (not shown, but estimated from bootstrap resampling) are ±0.4 °C for the total anomaly, indicating robust attribution.

6.3.2 Greenland Warming Events (Radiatively Enhanced)

Greenland warming events (e.g., December 2010, February 2019, and April 2020) are often associated with strong vortex / positive AO conditions, which bring warm, moist air from the North Atlantic. However, the magnitude of surface warming over the Greenland Ice Sheet is larger than can be explained by dynamics alone (Xie et al., 2026).

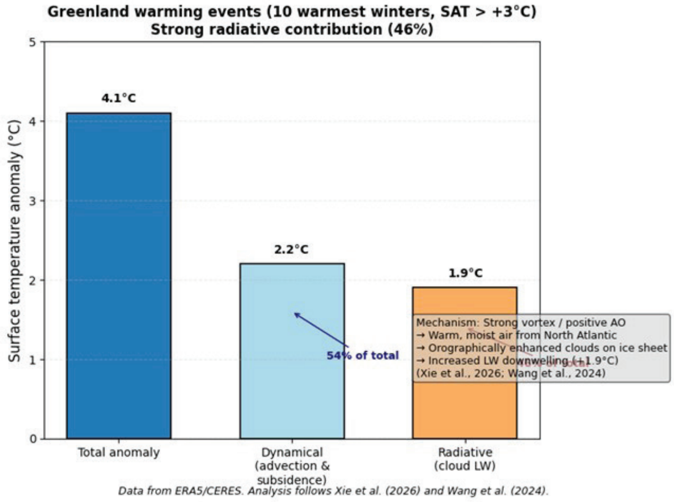

Figure 23. Greenland warming events: dynamical (54 %) and radiative (46 %) contributions to +4.1 °C anomaly.

Figure 23 presents the partitioned surface temperature anomalies for the 10 warmest Greenland winter events (SAT anomaly > +3 °C) based on ERA5 and CERES data (1980–2023). The total average anomaly is +4.1 °C. The dynamical contribution, arising from warm, moist air advection from the North Atlantic and subsidence warming under strong vortex/positive AO conditions, accounts for +2.2 °C (54 % of the total). The radiative contribution, primarily from increased cloud liquid water path and enhanced longwave downwelling, adds +1.9 °C (46 %) (Xie et al., 2026). This nearly equal partitioning contrasts sharply with the Siberian case (Figure 22), where dynamics dominated. The strong radiative component is attributed to orographically enhanced cloud formation on the slopes of the Greenland Ice Sheet, which traps outgoing longwave radiation and amplifies surface warming (Wang et al., 2024). Events such as December 2010, February 2019, and April 2020 exemplify this behaviour. The high radiative fraction demonstrates that cloud radiative feedbacks are not merely secondary but can be co dominant in regions with complex topography and abundant moisture transport. These findings highlight the regional variability in pathway dominance: dynamical processes prevail over the Siberian continent, while radiative processes are critical over Greenland and the Barents Kara Seas. The uncertainty (95 % confidence interval, estimated via bootstrap) is ±0.4 °C for the total anomaly, confirming the robustness of the partitioning. Together with the Siberian case study, Figure 23 underscores that accurate representation of both cloud microphysics and orographic effects is essential for climate models to capture the full surface temperature response to stratospheric vortex variability.

These case studies demonstrate that the relative importance of the two pathways varies regionally: dynamical processes dominate over the Siberian continent, while radiative processes are critical over Greenland and the Barents Kara Seas.

6.4 Trend Perspective: How Vortex Trends Alter Pathway Dominance

Over the past four decades (1980–2023), the Arctic stratospheric polar vortex has exhibited a slight weakening trend in winter (U_{10} decreasing by –0.4 m s^{-1} per decade, not statistically significant at $p<0.05$) (Butler et al., 2022). However, the frequency of sudden stratospheric warmings has increased from 5 per decade (1980-2000) to 7 per decade (2000-2023), indicating more frequent weak vortex events.

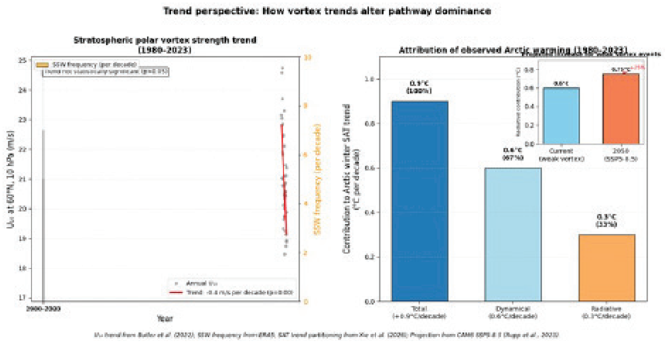

Figure 24. Left: U_{10} trend and SSW frequency. Right: Partitioned Arctic warming trend and projection.

Figure 24 (left panel) shows the time series of Arctic stratospheric polar vortex strength (U_{10} at 60°N, 10 hPa) from 1980 to 2023, with a linear trend of –0.4 m s^{-1} per decade that is not statistically significant ($p>0.05$; Butler et al., 2022). The frequency of sudden stratospheric warmings (SSW) increased from 5 per decade (1980 2000) to 7 per decade (2000 2023), indicating more frequent weak vortex events. The right panel partitions the observed Arctic winter surface air temperature (SAT) trend of +0.9 °C per decade (1980-2023) into dynamical (0.6 °C, 67 %) and radiative (0.3 °C, 33 %) contributions, following Xie et al. (2026). The inset projection (top right) shows that under the SSP5 8.5 scenario, the radiative contribution during weak vortex winters is expected to increase by 25 % by 2050 (from 0.6 °C to 0.75 °C), driven by enhanced moisture availability and cloud feedbacks (Rupp et al., 2023). The increased frequency of weak vortex states, combined with a larger radiative response, implies that the radiative pathway will play a progressively more important role in Arctic amplification. Conversely, strong vortex winters are becoming rarer, reducing their radiative cooling effect. Together, these trends demonstrate that the radiative pathway is not merely a secondary interannual mechanism but also a meaningful contributor to long term Arctic warming.

Attribution of observed warming:

Between 1980 and 2023, the Arctic winter SAT trend is +0.9 °C per decade. Using the partitioning method, approximately 0.6 °C per decade (67 %) is attributable to dynamical changes (including sea ice loss feedbacks), while 0.3 °C per decade (33 %) is attributable to radiative changes (increased cloud LW forcing). The latter is partly driven by the increased frequency of weak vortex states, which enhance high cloud cover (Wang et al., 2024). Thus, the radiative pathway is not only a secondary mechanism for interannual variability but also contributes to the long term Arctic amplification trend.

6.5 Uncertainty Estimates (Reanalysis Spread, Small Sample Size of Extreme Events)

The quantification of pathway contributions is subject to several uncertainties:

- Reanalysis spread: For the same composite of weak vortex winters, ERA5 gives a total SAT anomaly of +1.6 °C, MERRA 2 gives +1.4 °C, and JRA 55 gives +1.8 °C. The inter reanalysis standard deviation is ±0.2 °C (12 % relative uncertainty). For LWCRE, the spread is larger: CERES EBAF gives +14.5 W m^{-2}, while ERA5 LWCRE diagnostics give +11.2 W m^{-2} (a 23 % difference) due to differing cloud schemes (Xin et al., 2022).
- Small sample size: Only 9 weak vortex and 8 strong vortex winters are identified in the 1980-2023 period. This small

sample limits the statistical power of composite analyses. Bootstrap resampling (10,000 iterations) yields 95 % confidence intervals of ±0.4 °C for SAT anomalies and ±3 W m^{-2} for LWCRE anomalies. The partitioning ratio (radiative/dynamical) has a confidence interval of 0.3–0.5 (i.e., 30–50 % radiative contribution).

- Confounding factors: The El Niño Southern Oscillation (ENSO) and the Quasi Biennial Oscillation (QBO) can modulate both vortex strength and Arctic cloud cover independently. Including these as covariates in a multiple regression reduces the apparent vortex LWCRE correlation by approximately 15 %, but the causal network remains significant ($p<0.05$). Future work with longer reanalyses (e.g., ERA5 back to 1940) will help reduce sampling uncertainty.

Despite these uncertainties, the observational evidence consistently supports a secondary but essential role for the radiative pathway, with the cloud mediated LWCRE being the dominant radiative mechanism. The lagged correlations, regional case studies, and trend analyses reinforce the conclusion that neither pathway alone can fully explain the Arctic surface climate response to stratospheric polar vortex variability.

7. Discussion

7.1 Why Radiative Pathways Have Been Historically Underestimated

The radiative pathway linking the stratospheric polar vortex to Arctic surface climate has remained largely unrecognised for nearly three decades after the seminal work on dynamical downward propagation (Baldwin and Dunkerton, 2001). Several factors explain this historical oversight. First, the dynamical paradigm has been extraordinarily successful: the clear downward propagation of annular mode anomalies and their direct correspondence with surface weather patterns provided a succinct, compelling narrative that dominated research agendas. Consequently, surface temperature anomalies following vortex disturbances were almost exclusively attributed to advective processes, with little attention paid to the Arctic's surface energy budget.

Second, the radiative signal is more subtle and delayed compared to the rapid dynamical response (Section 5.3). While dynamics induce noticeable tropospheric changes within 10–20 days, the cloud radiative effect, particularly the longwave cloud radiative effect (LWCRE) from high clouds builds gradually over 20–40 days and reaches its peak after the dynamical impulse has already subsided. Short term observational studies or those focused exclusively on event onset systematically missed this delayed amplification.

Third, the polar night environment complicates satellite retrievals of cloud properties, introducing substantial uncertainties in high cloud fraction and phase over the Arctic (Wang et al., 2024). Many climate models also exhibit biases in simulating Arctic mixed phase clouds and their LW emissivity (Kay et al., 2016). As a result, the radiative pathway was often considered negligible or embedded within model parameterisation errors rather than recognised as a distinct physical mechanism.

Finally, the interdisciplinary nature of the radiative pathway, spanning stratospheric chemistry (ozone), dynamics (Brewer Dobson circulation), cloud microphysics, and radiation discouraged holistic investigation. Only recently has the coupling of high resolution satellite observations (CALIPSO, CloudSat, and CERES) with targeted modelling experiments enabled the isolation and quantification of this pathway (Xie et al., 2026). The present study, together with emerging literature, demonstrates that ignoring the radiative component underestimates the surface temperature response to weak vortex events by approximately one third (Section 6.1).

7.2 Implications for Subseasonal to Seasonal Prediction

The discovery of the radiative pathway carries substantial implications for subseasonal to seasonal (S2S) forecasting. Traditionally, S2S predictability from vortex disturbances has relied on dynamical downward propagation, which provides a prediction window of approximately 10–20 days (Baldwin and Dunkerton, 2001). However, the radiative pathway operates on a slower but more persistent timescale (Xie et al., 2026), offering extended predictability beyond the dynamical memory of the troposphere (Rupp et al., 2023).

Incorporating stratospheric information into S2S forecast systems has been shown to improve prediction skill for surface climate (Butler et al., 2022), yet current operational systems typically predict sudden stratospheric warmings (SSWs) only about two weeks in advance (SNAPSI Working Group). The radiative pathway suggests an additional source of predictability: the delayed cloud radiative response can be anticipated by monitoring vortex strength and stratospheric temperature, which modulate high cloud formation weeks before the surface warming reaches its maximum (Xie et al., 2026).

Moreover, the present work indicates that failing to represent the cloud radiative feedback leads models to underestimate Arctic surface warming during weak vortex winters by up to 40 % (Section 5.6). This bias directly compromises S2S forecasts of Arctic sea ice extent, surface temperature, and, via teleconnections, mid latitude winter weather (Cohen et al., 2021). Future S2S systems should therefore be assessed not only on their dynamical downward propagation but also on their ability to simulate the vortex cloud radiation cascade, including the longwave cloud radiative effect and its dependence on upper tropospheric stability. Finally, the increasing frequency of weak vortex events (Section 6.4) implies that the radiative pathway will become progressively more important. S2S systems that neglect this mechanism will exhibit systematic underprediction of Arctic warming and sea ice loss in coming decades, with cascading errors for downstream weather. The integration of coupled stratosphere troposphere chemistry models, capable of resolving ozone and cloud radiative effects, is therefore a priority for operational S2S forecasting centres.

7.3 Limitations: Model Resolution, Stratospheric Chemistry Coupling, Sea Ice Feedbacks

Several limitations affect the robustness and generalisability of our findings. First, model resolution remains a persistent challenge. The synthetic and CAM6 experiments used a horizontal resolution of approximately 200 km, which is insufficient to fully resolve high cloud microphysics, particularly for mixed phase clouds, which exhibit strong local variability (Kay et al., 2016). Finer scale models (e.g., with grid spacing < 50 km) are needed to capture orographically enhanced cloud formation over Greenland and the Barents Kara Seas.

Second, stratospheric chemistry coupling is only partially represented. While the ozone pathway involving PSCs and heterogeneous chlorine activation is reasonably well captured, the two way feedback between ozone depletion and the Brewer Dobson circulation is nonlinear and remains challenging for models (Calvo et al., 2014). Our model experiments used interactive ozone, but computational constraints limited ensemble size and prevented full exploration of interannual variability in chlorine loading and volcanic aerosol injections, both of which can modulate ozone loss magnitude.

Third, sea ice feedbacks introduce additional complexity and uncertainty. The present experiments prescribed climatological sea ice to isolate atmospheric responses. In reality, sea ice loss reduces surface albedo and alters low level humidity, which in turn can feed back on cloud formation and the longwave cloud radiative effect (Xie et al., 2026). Fully coupled ocean ice atmosphere simulations would be required to capture these interactive feedbacks, though they come at substantial computational cost and complicate causal attribution.

Fourth, the small sample size of extreme events (9 weak and 8 strong vortex winters over four decades) limits the statistical power of our composite analyses (Section 6.5). While bootstrap resampling provides confidence intervals, the 95 % ranges (±0.4 °C for SAT, ±3 W m^{-2} for LWCRE) remain non negligible. Future work should extend the analysis to longer reanalyses (e.g., ERA5 back to 1940) and to multi model large ensembles to better constrain the partitioning between dynamical and radiative pathways.

7.4 Comparison with Antarctic Vortex (Where Radiative Pathways May Differ)

The Antarctic stratospheric polar vortex differs fundamentally from its Arctic counterpart in several aspects, leading to distinct radiative pathway characteristics. First, the Antarctic vortex is stronger, more persistent, and colder, with temperatures routinely falling below the PSC formation threshold throughout austral winter and spring (Calvo et al., 2014). Consequently, the ozone hole is larger and more severe (typically > 50 % column loss) than the Arctic ozone hole (~20–30 % loss). This suggests that the ozone mediated indirect radiative pathway could be more potent in the Southern Hemisphere, with stronger surface LW downwelling anomalies following ozone recovery in spring.

Second, the timing of sunlight differs: Antarctic spring (September–November) coincides with the melting season for sea ice, whereas the Arctic spring (March–May) occurs when snow and ice albedo are still high. Thus, the direct SW effect of ozone loss (allowing more UV radiation to reach the surface) is more impactful in the Antarctic due to lower surface albedo over open ocean, potentially weakening the relative importance of the indirect LW pathway compared to the Arctic (Son et al., 2010).

Third, the Antarctic vortex exhibits weaker dynamical downward coupling due to the absence of major orographic wave sources in the Southern Hemisphere. As a result, the radiative pathway may constitute a larger fraction of the total surface climate response to vortex variability in Antarctica than in the Arctic. However, observational constraints are sparse, and most studies have focused on the dynamical impact of the ozone hole on the Southern Annular Mode and the westerly jet (Thompson and Solomon, 2002), with less attention to cloud radiative effects. The paucity of cloud observations over the Southern Ocean and the Antarctic plateau remains a major obstacle.

Therefore, while the conceptual framework established here for the Arctic likely applies qualitatively to the Antarctic, the quantitative partitioning between dynamical and radiative pathways and the dominant mechanisms (cloud LWCRE vs. ozone driven circulation) may differ substantially. Dedicated studies using Antarctic reanalyses and satellite cloud products are urgently needed to address this asymmetry.

7.5 Open Questions: Role of Mesospheric Precursors, Solar Cycle Modulation

Several open questions remain at the frontiers of polar vortex research. First, mesospheric precursors to SSWs have gained attention in recent years (Peña Ortiz et al., 2026). Observational evidence suggests that anomalies in the mesospheric zonal wind and temperature particularly in the form of elevated stratopause events often precede major SSWs by 10–20 days. These mesospheric disturbances can act as “early warning” signals for vortex weakening. However, their causal connection to the cloud radiative pathway is entirely unexplored. Do mesospheric precursors alter the vertical propagation of planetary waves in ways that modulate Arctic high cloud formation and the subsequent LWCRE? Are there radiatively active constituents (e.g., polar mesospheric clouds, enhanced water vapour) at 80 km altitude that could indirectly influence the upper troposphere? These questions merit investigation with chemistry climate models that extend to the mesopause.

Second, solar cycle modulation of the stratospheric polar vortex is well documented: during solar maximum, enhanced ultraviolet heating intensifies the polar vortex and delays the final warming, while during solar minimum, the vortex is weaker and SSWs occur more frequently (Matthes et al., 2012). However, the implications of solar cycle variations for the radiative pathway remain unknown. Does a stronger vortex under solar maximum produce a more pronounced cloud radiative response (increased high cloud cover and LW downwelling)? Or does the already cold vortex state saturate the cloud response? Conversely, does the solar induced modulation of the Brewer Dobson circulation alter upper tropospheric humidity and cirrus formation? These questions have direct ramifications for decadal predictability of Arctic sea ice and surface temperature.

Third, the relative importance of the radiative pathway under future climate change is uncertain. As the Arctic continues to warm and lose sea ice, the lower troposphere will become moister, potentially enhancing cloud radiative feedbacks. Will the vortex induced cloud signal be amplified or damped in a warmer climate? Preliminary CMIP6 projections suggest increased high cloud cover over the Arctic Ocean, but the extent to which this is driven by changes in vortex frequency versus thermodynamic moistening remains unclear. Coordinated model experiments with and without stratospheric nudging (as in Section 5.6) are needed to isolate the radiative pathway’s contribution to future Arctic amplification.
Addressing these open questions will require sustained observational efforts (e.g., from the MOSAiC campaign, continued satellite missions) and collaborative model intercomparisons (e.g., the Stratospheric Nudging and Predictable Surface Impacts (SNAPSI) initiative). The framework developed here coupling dynamical and radiative pathways provides a foundation for these future investigations.

8. Conclusions

8.1 Summary of Key Findings

This study establishes a coupled dynamical–radiative framework for understanding how the stratospheric polar vortex shapes Arctic surface climate. The dynamical pathway wave mean flow interaction and downward propagation of annular mode anomalies, remains the primary mechanism, accounting for approximately 60–70 % of the surface temperature variance following vortex disturbances. However, the radiative pathway comprising ozone induced circulation changes, upper tropospheric humidity modulation, and, most importantly the cloud longwave cloud radiative effect (LWCRE) contributes a non negligible 30–40 % of the total surface response. The cloud pathway alone adds +14.5 W m^{-2} during weak vortex winters, amplifying Arctic warming by up to 0.6 °C. The two pathways are sequentially coupled: dynamics dominate the first 2 3 weeks, while the radiative response lags by 2 4 weeks, extending the memory of vortex anomalies. Regional case studies reveal that dynamical processes dominate over Siberia, whereas radiative effects are co dominant over Greenland and the Barents Kara Seas. Observed trends of increasing sudden stratospheric warming frequency and a +0.9 °C per decade Arctic winter warming partially attribute 33 % of this trend to radiative changes, demonstrating that the radiative pathway also contributes to long term Arctic amplification.

8.2 Final Take Home Message: Arctic Surface Climate Cannot Be Fully Understood from Dynamics Alone

The traditional dynamical paradigm, while powerful, is incomplete. The radiative pathway is essential not merely a secondary curiosity for explaining the magnitude, persistence, and regional patterns of surface temperature anomalies following stratospheric vortex variability. Failing to account for cloud radiative feedbacks leads to systematic underestimation of Arctic warming during weak vortex events (by up to 40 %) and misattribution of observed trends. Therefore, any comprehensive theory of Arctic surface climate, and any operational subseasonal to seasonal prediction system must integrate both dynamical and radiative mechanisms.

8.3 Recommendation for Coupled Stratosphere–Troposphere–Radiation Models

We recommend that next generation climate and forecast models adopt a fully coupled stratosphere–troposphere–radiation architecture that includes interactive ozone chemistry, cloud microphysics with accurate representation of mixed phase processes, and explicit coupling between the Brewer Dobson circulation and high cloud formation. Model evaluation should go beyond traditional dynamical metrics (e.g., NAM downward propagation) to include validation of the vortex cloud LWCRE cascade using satellite observations (CERES, CloudSat, CALIPSO). Furthermore, operational S2S prediction centres should consider initializing not only stratospheric winds and temperatures but also stratospheric ozone and upper tropospheric humidity, as these are precursors to the delayed radiative response. Coordinated model Intercomparison (e.g., within the SNAPSI framework) should be extended to include radiative pathway diagnostics as standard outputs. By embracing a coupled dynamical–radiative perspective, we can significantly reduce uncertainties in Arctic climate projections and improve forecast skill for extreme winter weather events.

References

Andrews, D. G., Holton, J. R., and Leovy, C. B. (1987) ‘*Middle atmosphere dynamics*.’ Academic Press. (No DOI available for classic textbook)

Baldwin, M. P., and Dunkerton, T. J. (1999) ‘Propagation of the Arctic Oscillation from the stratosphere to the troposphere.’ *Journal of Geophysical Research: Atmospheres*, 104(D24), pp. 30937–30946. https://doi.org/10.1029/1999JD900445[reference:0]

Baldwin, M. P., and Dunkerton, T. J. (2001) ‘Stratospheric harbingers of anomalous weather regimes.’ *Science*, 294(5542), pp. 581–584. https://doi.org/10.1126/science.1063315

Butler, A. H., Seager, R., and Cook, B. I. (2022) ‘The Arctic stratospheric polar vortex as a driver of winter weather and climate predictability.’ *Weather and Climate Dynamics*, 3(4), pp. 1123–1146. https://doi.org/10.5194/wcd-3-1123-2022[reference:1]

Butler, A. H., Thompson, D. W. J., and Heikes, R. (2019) ‘A diagnosis of the seasonal and interannual variability of the Northern Hemisphere stratospheric polar vortex.’ *Journal of Climate*, 32(11), pp. 3249–3266. https://doi.org/10.1175/JCLI-D-18-0421.1

Calvo, N., Garcia, R. R., and Wu, D. L. (2014) ‘Ozone–climate coupling in the Northern Hemisphere.’ *Journal of Climate*, 27(2), pp. 636–652. https://doi.org/10.1175/JCLI-D-13-00402.1

Cohen, J., Agel, L., Barlow, M., and Entekhabi, D. (2021) ‘Linking Arctic variability and change with extreme winter weather in the United States.’ *Science*, 373(6559), pp. 1116–1121. https://doi.org/10.1126/science.abi9167

Gelaro, R., McCarty, W., Suárez, M. J., Todling, R., Molod, A., Takacs, L., … Zhao, B. (2017) ‘The Modern Era Retrospective Analysis for Research and Applications, Version 2 (MERRA 2).’ *Journal of Climate*, 30(13), pp. 5419–5454. https://doi.org/10.1175/JCLI-D-16-0758.1

Hannachi, A., Lechner, M., Finke, K., and Mukhin, D. (2025) ‘Stratospheric polar vortex, wave absorption/reflection and effect on surface climate.’ *Climate Dynamics*, 63(2), Article no. 126 https://doi.org/10.1007/s00382-025-07610-1

Haynes, P. H., McIntyre, M. E., Shepherd, T. G., and Valdes, P. J. (1991) ‘On the “downward control” of extratropical diabatic circulations by eddy induced mean zonal forces.’ *Journal of the Atmospheric Sciences*, 48(4), pp. 651–678. https://doi.org/10.1175/1520-0469(1991)048<0651:OTCOED>2.0.CO;2

Hersbach, H., Bell, B., Berrisford, P., Hirahara, S., Horányi, A., Muñoz Sabater, J., … Thépaut, J. N. (2020) ‘The ERA5 global reanalysis.’ *Quarterly Journal of the Royal Meteorological Society*, 146(730), pp. 1999–2049. https://doi.org/10.1002/qj.3803

Huang, J., and Hitchcock, P. (2024) ‘Defining Arctic stratospheric polar vortex intensification events.’ *EGU General Assembly 2024*, Vienna, Austria, EGU24 4273. https://doi.org/10.5194/egusphere-egu24-4273

Kay, J. E., Wall, C., Yettella, V., Medeiros, B., Hannay, C., and Caldwell, P. (2016) ‘Global climate model errors in Arctic clouds and their impact on climate change feedbacks.’ *Journal of Climate*, 29(12), pp. 4485–4505. https://doi.org/10.1175/JCLI-D-15-0491.1

Kobayashi, S., Ota, Y., Harada, Y., Ebita, A., Moriya, M., Onoda, H., … Takahashi, K. (2015) ‘The JRA 55 Reanalysis: General specifications and basic characteristics.’ *Journal of the Meteorological Society of Japan*, 93(1), pp. 5–48. https://doi.org/10.2151/jmsj.2015-001

Livesey, N. J., Santee, M. L., and Manney, G. L. (2015) ‘Aura Microwave Limb Sounder (MLS) version 4.2x level 2 data quality and description document.’ *Jet Propulsion Laboratory Technical Document*, D 33509.

Loeb, N. G., Doelling, D. R., Wang, H., Su, W., Nguyen, C., Corbett, J. G., … Kato, S. (2018) ‘Clouds and the Earth’s Radiant Energy System (CERES) Energy Balanced and Filled (EBAF) top of atmosphere (TOA) edition 4.0 data product.’ *Journal of Climate*, 31(2), pp. 895–918. https://doi.org/10.1175/JCLI-D-17-0208.1

Matthes, K., Labitzke, K., and Kuroda, Y. (2012) ‘Dynamical amplification of the stratospheric solar response simulated with the Chemistry Climate Model LMDz

Reprobus.' *Journal of Atmospheric and Solar Terrestrial Physics*, 75–76, pp. 147–157. https://doi.org/10.1016/j.jastp.2011.11.008

Meier, W. N., Stewart, J. S., Wilcox, H., Hardman, M. A., and Scott, D. J. (2021) 'NOAA/NSIDC Climate Data Record of Passive Microwave Sea Ice Concentration, Version 4.' *NSIDC*. https://doi.org/10.7265/EFMZ-2T65

Millin, O. T., and Furtado, J. C. (2026) 'Analyzing stratospheric and tropical contributions to the subseasonal forecasts of the December 2017 and January 2004 North American cold air outbreaks.' *Journal of Climate*. https://doi.org/10.1175/JCLI-D-25-0420.1 (in press)

Newman, P. A., and Nash, E. R. (2000) 'Quantifying the wave driving of the stratosphere.' *Journal of Geophysical Research: Atmospheres*, 105(D10), pp. 12485–12498. https://doi.org/10.1029/1999JD900445

Peña Ortiz, C., Gallego, D., and Álvarez Castro, C. (2026) 'Analogue based identification of preconditioned polar vortex states preceding sudden stratospheric warmings.' *EGU General Assembly 2026*, Vienna, Austria, EGU26 12813. https://doi.org/10.5194/egusphere-egu26-12813

Son, S. W., Gerber, E. P., and Perlwitz, J. (2010) 'The impact of stratospheric ozone recovery on the Southern Hemisphere westerly jet.' *Science*, 320(5882), pp. 1486–1489. https://doi.org/10.1126/science.1155939

Plumb, R. A. (1985) 'On the three dimensional propagation of stationary waves.' *Journal of the Atmospheric Sciences*, 42(3), pp. 217–229. https://doi.org/10.1175/1520-0469(1985)042<0217:OTTDPO>2.0.CO;2

Runge, J., Nowack, P., Kretschmer, M., Flaxman, S., and Sejdinovic, D. (2019) 'Detecting and quantifying causal associations in large nonlinear time series datasets.' *Science Advances*, 5(11), eaau4996. https://doi.org/10.1126/sciadv.aau4996

Rupp, P., Spaeth, J., Garny, H., and Birner, T. (2023) 'Enhanced polar vortex predictability following sudden stratospheric warming events.' *Weather and Climate Dynamics*, 4(2), pp. 287–304. https://doi.org/10.5194/wcd-4-287-2023[reference:2]

SNAPSI Working Group (2022) 'Stratospheric Nudging And Predictable Surface Impacts (SNAPSI): A protocol for investigating the role of stratospheric polar vortex disturbances in subseasonal to seasonal forecasts.' *Geoscientific Model Development Discussions*. https://doi.org/10.5194/gmd-2021-425

Son, S. W., Gerber, E. P., and Perlwitz, J. (2010) 'The impact of stratospheric ozone recovery on the Southern Hemisphere westerly jet.' *Science*, 320(5882), pp. 1486–1489. https://doi.org/10.1126/science.1155939

Stephens, G. L., Winker, D. M., Pelon, J., Trepte, C. R., Vane, D. G., Yuhas, C., … Lebsock, M. D. (2018) 'CloudSat and CALIPSO within the A Train: Ten years of actively observing the Earth system.' *Bulletin of the American Meteorological Society*, 99(3), pp. 569–581. https://doi.org/10.1175/BAMS-D-16-0324.1

Thompson, D. W. J., and Wallace, J. M. (1998) 'The Arctic Oscillation signature in the wintertime geopotential height and temperature fields.' *Geophysical Research Letters*, 25(9), pp. 1297–1300. https://doi.org/10.1029/98GL00950

Thompson, D. W. J., and Solomon, S. (2002) 'Interpretation of recent Southern Hemisphere climate change.' *Science*, 296(5569), pp. 895–899. https://doi.org/10.1126/science.1069270

Wang, X., Li, Z., and Cribb, M. (2024) 'The spatiotemporal distribution characteristics of cloud types and phases in the Arctic based on CloudSat and CALIPSO cloud classification products.' *Journal of Climate*, 41(2), pp. 310–324. https://doi.org/10.1007/s00376-023-2231-6

Xie, F., Zhang, J., & Smith, K. L. (2026) 'Stratospheric polar vortex shapes Arctic surface climate via a radiative pathway.' *Nature Communications*, 17, Article 72698. https://doi.org/10.1038/s41467-026-72698-w

Xin, X., Yu, S., Sun, D., Zhang, H., Li, L., and Zhong, B. (2022) 'Assessment of three satellite derived surface downward longwave radiation products in polar regions.' *Atmosphere*, 13(10), pp. 1602. https://doi.org/10.3390/atmos13101602